CODEN:LUTEDX/(TEIE-5522)/1-71(2024)

Industrial Electrical Engineering and Automation

Position tracking of optical modules in multidirectional network cameras by using ultrasonic waves

Gustaf Waldén
Linnéa Rydberg

Division of Industrial Electrical Engineering and Automation
Faculty of Engineering, Lund University

Position tracking of optical modules in multidirectional network cameras by using ultrasonic waves

Faculty of Engineering, Lund University

Division of Industrial Electrical Engineering and Automation

LUND UNIVERSITY

LTH

FACULTY OF ENGINEERING

Gustaf Waldén & Linnéa Rydberg

Examiner: Fran Marquez

15th September 2024

Abstract

In products with multiple, movable components it is often important to know the position of them. Such an example is to localize the different optical modules used within a multidirectional surveillance camera. This thesis explores the feasibility of using ultrasound distance-measuring technology for that particular application. Various methods and technologies were examined before developing a concept that utilises commonly used piezoelectric transducers in conjunction with time of flight distance measurements.

A prototype was constructed based on this concept, aiming to investigate the limitations and capabilities of this approach. In parallel, a signal processing algorithm was implemented to acquire accurate distance measurements. The prototype's accuracy in determining distance and position was thoroughly tested, revealing a positional accuracy within $\pm 8^{\circ}$. The performance of the prototype was evaluated, highlighting its strengths and limitations. Finally, recommendations for future work are proposed to further enhance the system's accuracy and reliability.

Sammanfattning

I produkter med flera, rörliga komponenter är det viktigt att veta postitionen på dessa. Ett sådant exempel är att lokalisera de olika optiska modulerna i en multidirektionell övervakningskamera. Denna masteruppstats undersöker möjligheten att använda ultraljudsteknik för avståndsmätning anpassad till just denna applikation. Olika metoder och tekniker undersöktes innan ett koncept utvecklades. Konceptet bestod av en kommersiellt utbrädda piezoelektriska ultraljudsgivare, i kombination med *Time of flight* teknik.

Baserat på denna metod byggdes en prototyp för att undersöka konceptets begränsningar och möjligheter. Parallellt implementerades en signalbehandlingsalgoritm för att erhålla noggranna avståndsmätningar. Prototypens noggrannhet när det gäller att bestämma avstånd och position testades noggrant, vilket visade en positionsnoggrannhet inom $\pm 8^{\circ}$. Prototypens prestanda utvärderades, och dess styrkor och begränsningar lyftes fram. Slutligen föreslogs rekommendationer för ett framtida arbete med att ytterligare förbättra systemets noggrannhet och tillförlitlighet.

Acknowledgements

Writing this thesis has been a very educative task with much knowledge and experience gained from it. We have been challenged to learn and implement new techniques previously unknown to us. It has also been very interesting to work on an industry based task, preparing us further for the work life as engineers and shrinking the gap between the academic world and the industry.

We would like to extend a thank you to our industrial supervisors from Axis Communications AB: Jimmy Lovén, Anders Wahlbom, and Roger Nilsson, for their invaluable support and guidance throughout the project. Also, a thanks to the team of MCP Electronics at Axis for making our time at the company an unforgettable and enjoyable experience.

We would also like to express our gratitude to our academic supervisor, Johan Björnstedt, for giving good advice and support regarding the project. Additionally, a thanks to Gunnar Lindstedt for providing knowledge within ultrasound in particular.

We would also like to thank our friends and families for giving us support throughout the time this thesis has been written.

Finally, we would like to thank each other for the excellent cooperation throughout the project. The work in this thesis has been divided equally between both authors.

Acronyms

ADC Analog to Digital Converter

CAD Computer-aided design

CMUT Capacitive micromachined ultrasonic transducers

DFT Discrete Fourier Transform

DMA Direct Memory Access

DSP Digital signal processing

EMI Electromagnetic Interference

FFT Fast Fourier Transform

FoV Field of view

FPU Floating Point Unit

IC Integrated Circuit

IDE Integrated Development Environment

MCU Microcontroller Unit

MEMs Micro-Electro-Mechanical systems

NFL Near-field length

p-p Peak to peak

PMUT Piezoelectric micromachined ultrasonic transducer

PVDF Polyvinylidene fluoride

PWM Pulse-width modulation

SPL Sound Pressure Level

TDoA Time Difference of Arrival

ToF Time of Flight

Contents

1 Introduction

1.1 Background

Network cameras have proven to be invaluable tools for enhancing security and video surveillance. Through the provision of real-time intelligence, cameras contribute to the establishment of an environment characterized by increased security and operational efficiency. Panoramic cameras offer extensive coverage of wide areas, integrating multiple optical modules into a single product. A multidirectional camera with four optical modules is illustrated in Figure 1.1. An optical module is the component that houses the optics and image sensors. The modules can be positioned anywhere on a 360° rail, providing great flexibility. It is essential to be able to track the position of the optical modules during installation, as otherwise they can run into each other and possibly harm the mechanics or lead to other undesired events.

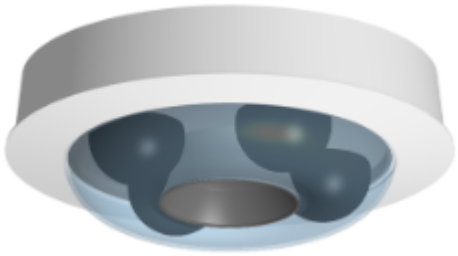

Figure 1.1: Illustration of a multidirectional camera, with four optical modules [1]. Reprinted with permission.

As of now, the position tracking of the optical modules could be done through an indirect estimation. When calibrating the modules, it is both time consuming and the position might also drift over time. Consequently, this leads to an inaccuracy of the absolute position, which in turn leads to the need of a recalibration of the module.

1.2 Goal

The aim of this master thesis was to investigate and introduce a direct method to track the position of optical modules in multidirectional network cameras

by utilising ultrasonic waves and deliver a proof of concept. Ultrasonic measurement was investigated to see if it would provide a good distance accuracy, while made out of affordable components. In particular, the thesis developed a concept prototype, including a processing method and algorithm for distance measurement customized for application. The goal was to get a working prototype and provide a foundation for future implementation in the product.

1.3 Product requirement specification

For the prototype to be implemented in a surveillance product it needs to meet the requirements of operating temperature of $-40°$ to $+70°$ C. The prototype shall provide a maximum position deviation of $\pm 0.5°$. Finally, it must also be able to determine a position in an environment with obstacles, e.g. cables which have come loose.

1.3.1 Concept

A concept was developed in the early stages of the project on how to utilize ultrasound and obtain the position of the optical modules within the camera. Examination of the mechanics of the camera in Figure 1.1, revealed an empty void between the existing operating mechanics and the surface where the camera is mounted. By allowing the optical modules to project their position from the rail into the void, the ultrasonic transducer can be mounted and operated in the void without interference from other electronics or mechanics. The working space for the prototype could therefore be simplified into a disc with the height of the void. The projection of the modules and the working space is illustrated in Figure 1.2.

As the optical modules move along the circular rail, the transducers fixed to the modules follow and a new position can be measured. The positions of the modules are therefore not always positioned as in Figure 1.2. The movement of a module is only restricted by the position of the neighbouring modules as a collision between two is unwanted.

The concept is founded on the fact that the ultrasonic waves have an unhindered path in between the transducers. The concept includes two ultrasonic transmitters and one receiver for each optical module, serving as pitch and catch modules. The ultrasonic distance measurement is derived from the propagation time method, commonly known as Time of Flight (ToF). The reason this was chosen among others was that the implementation of it was expected to be a straight forward process, not to be confused with simple, and also be the one with the highest probability of reaching a result. The method

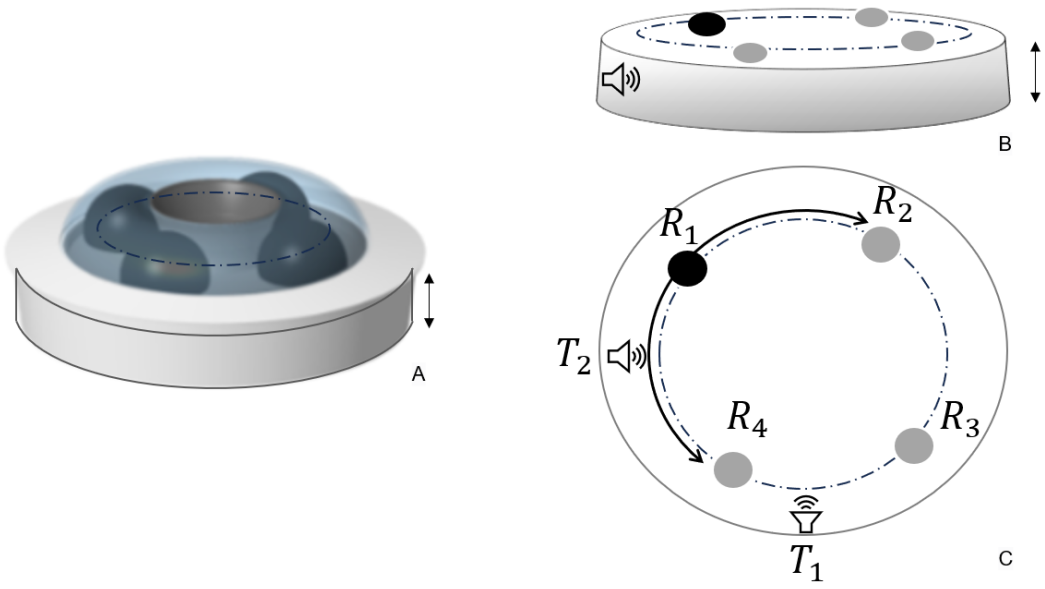

Figure 1.2: The working space of the concept is seen in A and B. Two ultrasonic transmitters, sonic icons, and four positions of the optical modules, the circles. The movement of receiver R1 is exemplified in the subfigure C, but in reality all four receivers can also move around. Subfigure A is reprinted and reworked with permission.

is also the one that requires the least amount of components.

1.4 Delimitations

This thesis aims to develop a proof of concept rather than a final prototype that is ready to be implemented into a product. Consequently, this thesis focuses on one technique of distance measurement and identifying the variables with good accuracy, rather than evaluating several feasible techniques.

As the goal is to develop a proof of concept the radius of the prototype is not based upon a specific product, but rather arbitrary dimensions of a typical surveillance camera. Multidirectional cameras come in various designs, thus varying in dimensions. Moreover, the concept was reduced to a two dimensional measuring problem, with transmitters and receivers operating on the same radius. This introduced blind spots where the receiver could not be positioned where the transmitter needed to be fixed. Hence, the goal was not to cover the full 360° range to narrow the scope of the work. That was left for future development.

1.5 Methodology

The philosophy of development in this thesis can be described as a linear process with a mindset of moving forward when possible. This methodology prioritizes progression over optimization at each stage. Upon achieving a subgoal, the focus shifts immediately to the subsequent task instead of improving and optimising the parameters to attain the optimal solution for the current subgoal. Commonly, this is known as "*good enough*". This strategy ensured continuous forward momentum in the development cycle. Improvements would only be made if time remained after the prototype was operational.

The process of development was characterised by creating a prototype that is both a feasible solution to continue development of, and also creating a prototype that would be economically viable to implement in a camera.

1.6 Disposition of the report

General knowledge about ultrasound, followed by additional theory that has been utilised in this project is presented in chapter 2. The work done in this thesis is divided into two phases. The first phase includes the work that relates to hardware, such as circuits and components, and is found in chapter 3. The second phase, found in chapter 4, explains the work related to signal processing, the software developed and calibration of parameters made to get a better distance measurement. The test to evaluate the performance is described in chapter 5. The resulting distance measurements are presented and discussed in chapter 6. In chapter 7 potential improvements to the developed concept are presented and discussed. Some of which were never part of the scope of the project from the beginning, and some of it had to be left out due to time constraints.

2 Theoretical Background

This chapter explains the relevant calculations and theory, as well as presents the various components and techniques used in the project.

2.1 Angle calculation

To determine the position of the optical modules in a three dimensional working space, trigonometry is applied. Assuming a reference system, you can calculate the position of a point based on its relative position to at least two other known points. Two points are located perpendicular to one another with a known distance on a set coordinate system, radius r_1. They have the fixed coordinates $T_1 : (-r_1, 0, 0)$ and $T_2 : (0, -r_1, 0)$. The unknown point is located somewhere on the circle with the known radius r_2 and offset h in the z-direction, with the unknown angle θ, illustrated in figure 2.1. The coordinate for one receiver can be expressed as $R_1 : (r_2 cos\theta, r_2 sin\theta, h)$.

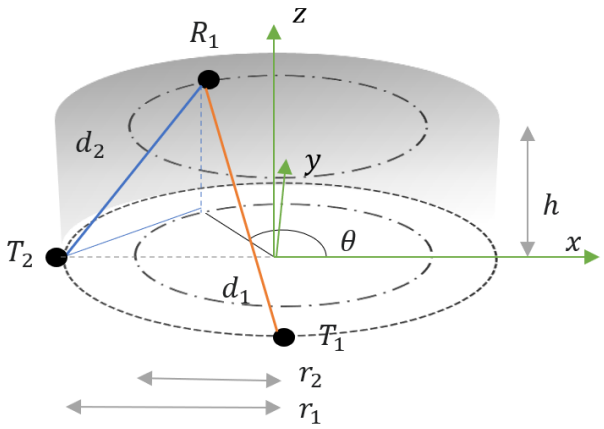

Figure 2.1: The image depicts the parameters r_1, respectively r_2, in the equations to calculate to relative angle of the receiver. Transmitters are marked with T and receiver with R.

The distance between the unknown and the two known points is called d_1 and d_2. With the preceding data, the subsequent equations can be derived, incorporating the Pythagorean theorem where d_1 is expressed as

$$(r_2 cos\alpha)^2 + (r_1 + r_2 sin\alpha)^2 + h^2 = d_1^2, \tag{2.1}$$

and accordingly d_2 is expressed as

$$(r_1 + r_2 cos\varphi)^2 + (r_2 sin\varphi)^2 + h^2 = d_2^2. \tag{2.2}$$

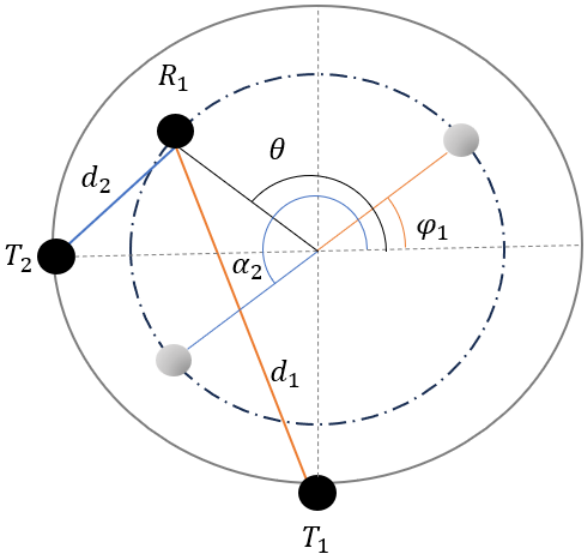

Figure 2.2: Two potential positions at φ_1 and α_2, but only one feasible position for R_1 at θ, determined from the two distance readings, d_1 and d_2.

Both φ and α can be derived to two potential angular solutions

$$\varphi_1 = cos^{-1}(\frac{d_2^2 - r_1^2 - r_2^2 - h^2}{2r_1 r_2}); \qquad \varphi_2 = 2\pi - cos^{-1}(\frac{d_2^2 - r_1^2 - r_2^2 - h^2}{2r_1 r_2}), \tag{2.3}$$

$$\alpha_1 = sin^{-1}(\frac{d_1^2 - r_1^2 - r_2^2 - h^2}{2r_1 r_2}); \qquad \alpha_2 = \pi - sin^{-1}(\frac{d_1^2 - r_1^2 - r_2^2 - h^2}{2r_1 r_2}), \tag{2.4}$$

but only one where $\theta = \alpha = \varphi$. Given the two distances, it exists only one unique solution.

For a two dimensional working space, $h = 0$. Additionally if the two radius, $r_1 = r_2 = r$, equations 2.1 through 2.4 can simplified to depend on only one parameter r.

2.2 Ultrasound physical properties

Ultrasound refers to sound waves with frequencies beyond the range of human hearing, usually defined as all sound with a frequency above 20 kHz up to several GHz. This section will explain the physical background and ultrasonic properties in air.

2.2.1 Propagation

Ultrasound falls under the category of mechanical waves, more specifically the theory of acoustic waves can be applied. A mechanical disturbance can travel through a medium due to its elastic properties. Acoustic waves are a type of longitudinal elastic wave that propagates through a medium by compression and decompression. In detail, the particles in air oscillate and exchange the kinetic energy with potential energy stored due to compression [2].

Attenuation refers to the reduction in amplitude of the ultrasonic beam as it travels through the medium. In air, the attenuation is mainly due to diffraction, but absorption is also a contributing factor [3]. The area covered by the wavefront increases with the distance from the source. Consequently, the pressure amplitude decreases. The maximum Sound Pressure Level (SPL) is always along the center line acoustic axis.

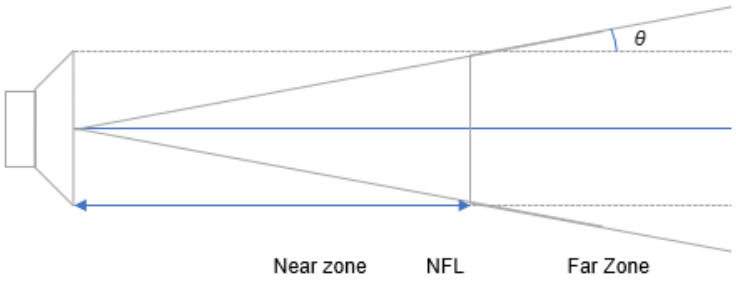

Figure 2.3: The piston model with near zone and far zone being separated by the near field length, NFL. The directivity is indicated by the beam angle.

The sound propagation for a transducer can be described with the piston model, illustrated in Figure 2.3. The equivalent source of the piston model is letting plane parallel waves, with the wavelength λ, pass through a circular opening with the diameter D. The sound beam zones within the piston model can be divided in two zones; near zone and far zone. Within the Near-field length (NFL), also called the near zone, the pressure amplitude of the sound wave varies with a circular symmetry centered on the beam axis [2]. The end of the near zone is defined by equation 2.5 as

$$NFL = \frac{D^2}{4\lambda}. \tag{2.5}$$

In the far zone, destructive interference does not occur. This results in the maximum value in the central axis of the sound beam. Instead the beam diverges with the angle θ. The angle of diverges is given by equation 2.6:

$$\sin\theta = K\frac{\lambda}{D}, \tag{2.6}$$

where K is a constant with different values within the edge beam spread. When the sound intensity drops by half, the K factor is 0.56. The beam intensity reaches its first minimum, where the intensity falls to zero, when K is 1.22. The higher the frequency of a crystal, the less the sound wave spread out contributing to a lower beam angle.

2.2.2 Impedance and reflection

Acoustic impedance Z of a material is a product of its density ρ and its acoustic velocity c:

$$Z = \rho \cdot c. \tag{2.7}$$

The acoustic impedance is a characteristic that determines transmission and reflection at a boundary of two media [3]. A difference in impedance leads to energy losses in SPL due to some of the wave being reflected, and some being transmitted and propagated into the material. The fraction of the energy that is reflected can be calculated according to Equation 2.8

$$R = (\frac{Z_2 - Z_1}{Z_2 + Z_1})^2, \tag{2.8}$$

where R is the reflection coefficient, Z_1 and Z_2 are the acoustic impedances of the first and second media respectively, through which the wave propagates.

2.2.3 Speed of sound

Sound stands under the influence of several parameters which affects its properties. The material through which sound waves propagate significantly affects the speed. Another parameter that must be taken into account when calculating the speed of sound is the temperature of the medium. When referring to the speed of sound in air, a common number mentioned is 343 m/s. Although, that is only true for 20°C. The speed of sound in air can be calculated as

$$v = 331\sqrt{1 + \frac{T}{273}}, \tag{2.9}$$

where v is the speed of sound in meters per second and T is the temperature in degrees Celsius [4, Ch. 17.2].

2.3 Ultrasonic area of use

This section will present some of the fields where ultrasound technology is applied.

2.3.1 Diagnostic

Ultrasound is one of the most widely used non-invasive imaging techniques for medical diagnostics. Ultrasound imaging, or sonography, is used as an inter-

active imaging technique in which the operator holds the ultrasound probe in contact with the patient and observes images of internal anatomy in real time. Sonography is based on echoes generated by the reflection of ultrasound waves at tissue boundaries and scattering from small irregularities within tissues. Additionally, the Doppler effect can be used to detect the motion of blood in arteries, veins and in the heart [2].

2.3.2 Ultrasonic testing

Ultrasound is not only used within the medical sector, it has a variety of applications across industry. Ultrasonic testing is a non-destructive testing technology that is ideal for detecting defects, cracks and cavitation within a part without damaging the material. Finding these flaws is crucial as they could potentially weaken a construction and thus prevent failure for the component being inspected. For example, ultrasonic testing is used for inspection of corrosion, thickness measurements and testing for discontinuities in welds [5].

2.3.3 Ultrasound in nature

Echolocation is biological adaptation found in certain species of animals. The technique allows animals to navigate their environment, locate prey and obstacles using ultrasonic sound waves. Because of compatibility difficulties due to differences in specific acoustic impedance, propagation in air causes amplitude of the waves to decrease. Among the most adept practitioners of echolocation in air are bats.

Bats have evolved a distinct and complex form of echolocation to navigate and hunt in their nocturnal habitats. Bats emit high-frequency calls through their throats while in flight. The features of the sonar vocalizations change as the bat approaches the target [6]. By either changing the frequency or by doing range-dependent adjustments, the different bat species have a complex set of adaptive behaviours in response to dynamic acoustic information. Bats can accurately locate prey, avoid obstacles, and navigate in complete darkness. Similar the way bats navigate, this project uses ultrasound to track the optical modules in air.

2.4 Ultrasonic transducer

A transducer is a device that converts one form of energy into another. In context of ultrasound, the transducers converts electrical energy into mechan-

ical energy in order to transmit a sound wave, and vice versa to receive the ultrasonic sound. Due to differences in acoustic impedance in air and solid materials, there are commonly two transducer principles used, the piezoelectric and the electrostatic.

2.4.1 Piezoelectric Transducers

The piezoelectric transducer is based on the piezoelectric crystal. The piezoelectric crystal expands or contracts when a positive or negative external voltage is applied. Conversely, the elements generate voltages when exposed to mechanical oscillation. The phenomenon is based on that the polarized grains align themselves with an electric field when it is applied across the material. The alignment will result in induced dipoles, and a change in the dimensions of the material [2]. The piezoelectric effect is illustrated in 2.4.

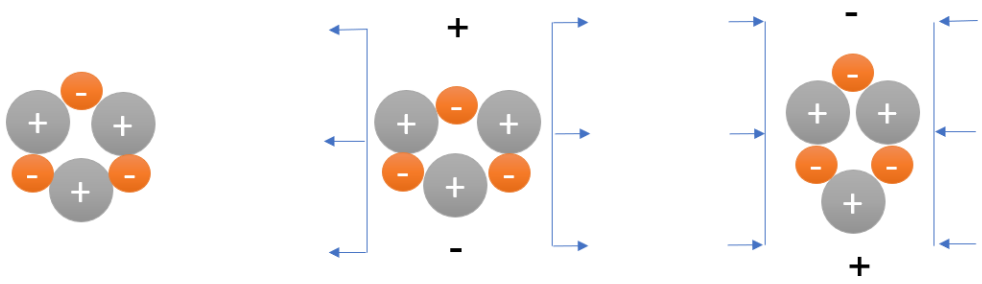

Figure 2.4: A schematic illustration of the piezoelectric effect.

Besides the high electrical to mechanical efficiency, another beneficial characteristic is the low supply voltage. On the other hand, piezoelectric transducers have a narrow bandwidth and high impedance. In case of bursting wave into air, the impedance difference reduces the SPL achievable. It implies that only a small part of the energy will leave the element and limits the signaling range, for a given sound noise ratio [7]. Furthermore, the resonance dynamics in a piezoelectric element will cause the crystal to oscillate after an pulse, the so called ringing time [3].

There are two types of drivers for piezoelectric transducers, dependent on the transducer's maximum drive voltage: transformer and direct drive [8]. Transformer drive is superior for both short and long range performance and for transducers that require larger driver voltage. The transformer drive allows for a large excitation voltage and supports the use of additional external matching components to dampen the ring decay energy. With the direct drive, the transducer is supplied with pulses directly from the source. Direct drive does

not perform as well because of the longer ring-decay time and therefore hinders the minimum range capability. On the other hand, the direct drive does not require as many components and is therefore both smaller and cheaper than the transformer driver.

A piezoelectric element provides a wide range of possibilities for characteristic modification in production. The thickness of the active element is determined by the desired frequency of the transducers, expanding up to the MHz range. The higher the frequency, the thinner the active element. The beam spread depends on the frequency and the diameter of the transducer. The transducers can be either open top or closed top. The closed-top transducer has a sealed housing and is suitable for outdoor environments, but needs a larger driving voltage. In an open-top transducer, the piezoelectric membrane is directly coupled to air for increased receiver sensitivity.

Besides crystal, there are other materials with piezoelectric properties.
Polyvinylidene fluoride (PVDF), is a piezoelectric polymer that has been developed into an ultrasonic transducer [7]. In comparison, the PVDF has a broader bandwidth but requires a high polarization voltage. Piezoelectric transducers are a popular conventional sensor that has become cost-effective for large scale production.

2.4.2 Electrostatic transducers

Electrostatic transducers are based on the principle of electrostatic force between two conductive electrodes [9]. The electrostatic elements are constructed of one conductive plate, an insulator, and a thin conductive membrane. A cavity is formed when the grooved plate is layered by the membrane. The membrane and the plate serve as biased electrodes, charged by a DC voltage and separated with the insulator, see Figure 2.5. When an alternating voltage is applied, the electrostatic force will cause the membrane to vibrate. The frequency is dependent on the cavity size and the stiffness of the membrane. Conversely, the membrane will start vibrating when subjected to ultrasonic waves due to a change in capacitance. The electrostatic transducer has a somewhat lower sensitivity but has the advantage of no resonance characteristic compared to piezoelectric elements. This makes it less sensitive to noise and facilitates the signal processing due to no ringing time. Electrostatic elements have a wide bandwidth. Higher frequency ranges are difficult, due to the decreased amplitude. Additionally, a high biased voltage makes it harder to design circuits.

The electrostatic sensors are less established and less common than the piezoelectric elements, which also affects their price.

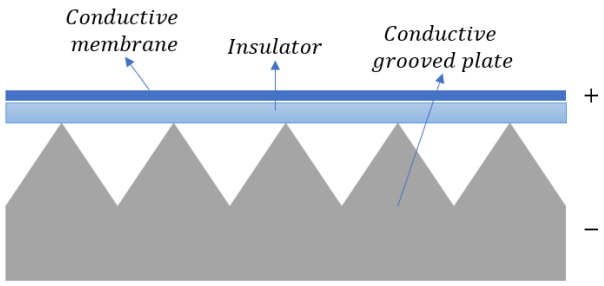

Figure 2.5: The functional principle for an electrostatic transducer with a two charged conductive electrodes separated by in insulator.

2.4.3 MEMs

Micro-Electro-Mechanical systems (MEMs) is a fairly new technology that integrates mechanical and electrical components into miniature devices. With high precision and unique small size, the demand for MEMs devices increases. MEMs ultrasonic transducers can both be piezoelectric and electrostatic.

Capacitive micromachined ultrasonic transducers (CMUT) is based on electrostatic technology, and have recently emerged as an alternative to conventional piezoelectric transducers [10]. The MEMs technology allows the CMUT to be constructed of a large number of membranes with precise dimensions fabricated in layered arrays onto silicon. This enables high transduction efficiency and sensitivity. Additionally, it enables higher frequency applications, operating in the MHz range in air.

The Piezoelectric micromachined ultrasonic transducer (PMUT) consists of a thin piezoelectric layer on a flexible membrane. PMUT offers an increased bandwidth and operation at lower voltages.

2.5 Distance measurements

Ultrasonic distance measurement methods are based upon ToF. The principle is that the distance is directly proportional to the time elapsed since the ultrasound was transmitted to the waves received. The distance reading can either be done by letting a transmitted signal be reflected on an object and then receive the echo, the so called *pulse-echo* method. The signal can also be received without reflection, also known as the *pitch-catch* method. With a known velocity c, the distance d can be calculated by one of the following equations:

$$pitch\text{-}catch : d = c \cdot t_{ToF}; \qquad echo\text{-}pulse : d = \frac{c \cdot t_{ToF}}{2}. \tag{2.10}$$

The transmitted signal that propagates through air attenuates with distance. Additionally, background noise causes the signal to change. The received signal can therefore be expressed by the following equation:

$$r(t) = \gamma p(t - t_{ToF}) + n(t), \tag{2.11}$$

where $r(t)$ is the received signal, γ is an attenuation factor due to propagation. $p(t)$ is original transmitted signal and $n(t)$ is the noise added to the signal.

Closely related to ToF, Time Difference of Arrival (TDoA) is a technology used for investigating the localization of a source. TDoA is based on spatially separated receivers acquiring the same emitted signal but with a slight time delay [11]. The two received signals can then be expressed, as an extension of Equation 2.11, as

$$r_1(t) = \gamma p(t - t_{ToF}) + n_1(t). \tag{2.12}$$

and the second signal which accounts for the time difference of arrival, τ, as

$$r_2(t) = \gamma p(t - t_{ToF} - \tau) + n_2(t). \tag{2.13}$$

2.5.1 Threshold method

One of the possible ways to detect that an ultrasonic wave has reached the receiver is by implementing threshold detection. As the sound wave approaches the receiving transducer, it will start to oscillate with an increasing amplitude. Once the oscillation reaches a given threshold, the sound wave is detected. ToF is computed by knowing when in time the pulse was sent and when it was received. Depending on the threshold level, an offset error will be introduced, see figure 2.6.

A downside with this method is that it suffers from poor resolution since it is dependent on the magnitude of the received signal [12]. On the other hand, it is a simple low cost solution that could be implemented electrically with a comparator, without the need for signal processing.

2.5.2 Cross-correlation method

In contrast to the threshold method, cross-correlation is independent of the magnitude of the signal, but rather dependent on the waveform of the received signal when sound is to be analysed. When there is a possibility to know what to look for in a set of data it is possible to determine the similarity across the

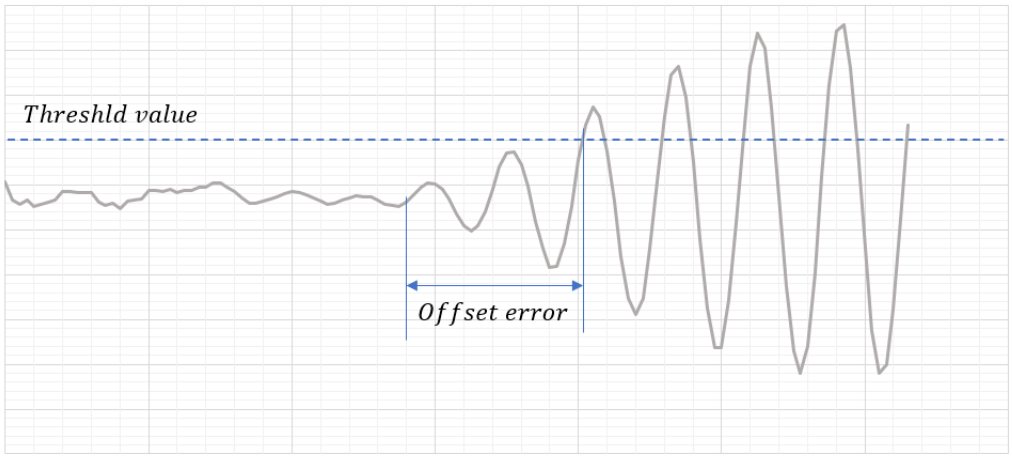

Figure 2.6: Time estimate with threshold method with an offset error.

collected data and the reference data. In terms of ultrasound, this is done by comparing the reference wave at every possible combination with the longer measurement specific wave. The output of the calculation generates an array of correlation values. At some point in the array, there will be a peak in the correlation data, if there is a match, which indicates where the set of data is the most similar to the reference [13].

The following is an example of cross-correlation in the discrete time domain of a sampled signal. For two functions $f = [1\ 2\ 1]$ and $g = [1\ 2\ 1]$ the task is to compare and decide when they match each other, when they correlate the most. One of the functions is frozen in time, and the other one is shifted one element at a time from right to left. Cross-correlation is done by element-wise multiplying the two functions and sum the result. Below is an example of that.

$$\begin{matrix}[1 & 2 & 1] & & \\ & [1 & 2 & 1]\end{matrix} \qquad \begin{matrix}[1 & 2 & 1] & \\ & [1 & 2 & 1]\end{matrix} \qquad \begin{matrix}[1 & 2 & 1] \\ [1 & 2 & 1]\end{matrix}$$

$$1 \cdot 1 = 1 \qquad 2 \cdot 1 + 1 \cdot 2 = 4 \qquad 1 \cdot 1 + 2 \cdot 2 + 1 \cdot 1 = 6$$

If the example would have continued two more steps the result of the correlation array would be $fg_{corr} = [1\ 4\ 6\ 4\ 1]$. The output array of cross-correlation tells when the two functions correlated the most at the highest value. In the example, it would be the point in time where the output was 6.

2.5.3 Phase shift

An additional principle to detect the ToF, is by observing the phase shift. This method reduces the need for a fast sampling rate and may therefore increase the accuracy [3]. This method relies on continuously transmitted carrier waves with known frequency. The received signal then can be expressed as a complex representation of that frequency, with an amplitude and a phase. Additional frequencies from noise can therefore be filtered away. The distance can then be evaluated by comparing the transmitted signal to the received one

$$t_{ToF} = (N + \frac{\beta}{2\pi})/f, \tag{2.14}$$

where N is the integer of wavelengths, β is the phase shift and f is the frequency of the transmitted wave [12].

2.5.4 Advantages of ultrasound measurement

Ultrasonic technology provides a wide range of advantages when used for measuring distance. In the spectrum of electromagnetic waves, both light and microwaves can be applied for distance reading using ToF. However, with the waves traveling with the speed of light, the delay time becomes significantly reduced compared to ultrasonic waves traveling with the speed of sound. Consequently, the system needs to become more expensive due to the requiring higher sampling rates. Ultrasonic measurement provides a feasible compromise between cost and resolution and can be applied for a broad distance range. Ultrasonic measurement provides the benefits of being harmless for humans, as well as insensitive towards dust and Electromagnetic Interference (EMI). In addition, the distance reading is unaffected by light, optically transparent surfaces and colors.

2.6 Ultrasonic ranging module

Ultrasonic range sensors detect objects and are used to measure a distance. Two modules, HC-SR04 and SRF004, were studied in order to learn more about distance measurement. Both sensors use threshold detection of a receiving echo. The modules include a transmitter, a receiver, and a control circuit. The distance sensors emit 40 kHz ultrasound by an 8-cycle sonic burst to measure objects in their path by detecting its echo. The HC-SR04 module has a range between 2 cm, up to 4 m, and the ranging accuracy can reach 3 mm.

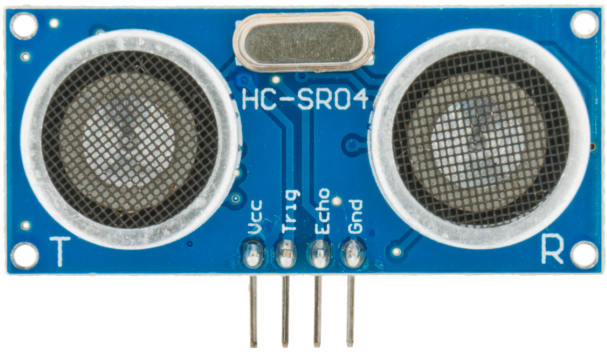

Figure 2.7: HC-SR04 ultrasonic distance sensor [14]. Reprinted with permission.

2.6.1 MAX232

MAX232 is an Integrated Circuit (IC) by Maxim Integrated Products that converts signal from RS232 to serial port signal for use on transistor–transistor logic compatible digital circuits [15]. The MAX232 is a dual transmitter and dual receiver that is typically used to convert the RX, TX, CTS, and RTS signals. However, this component is integrated into the SRF004 distance sensor as a charge pump circuitry. The MAX232 is beneficial since it can convert 0/3.3 V signal to -10/10 V signal on a small physical footprint. Additionally, it provides both positive and negative 10 V power supply from a 5 V supply.

2.7 Development board

STM Nucleo-64 development board with STMF401RE Microcontroller Unit (MCU) is produced by STMicroelectronics and is a member of the STM32F4 series of high performance MCU [16]. The board has an integrated ST-LINK debugger, and is connected to a computer via USB.

This MCU is based on the ARM Cortex M4 processor, which allows for Digital signal processing (DSP) instructions and operates at a maximum clock frequency of up to 84 MHz. The MCUs has hardware support for Floating Point Unit (FPU) which allows fast operations with floating point units. Additionally, the processor features up to 512 KB of Flash memory and includes a 96 KB of SRAM for data storage.

The MCU is equipped with one 12-bit Analog to Digital Converter (ADC) with up to 16-channels and a general purpose Direct Memory Access (DMA). The controller holds up to 11 timers, including one advanced control timer, and several general purpose inputs/outputs channels.

Figure 2.8: STM Nucleo-64 development board of model STMF401RE [17]. Reprinted with permission.

STMicroelectronics provides comprehensive software tools for developing applications. The development board supports a wide choice of Integrated Development Environment (IDE)s, including STM32CubeIDE which is specially designed for STM32 microcontrollers. Additionally, STM32CubeMX is a graphical configuration tool that configures peripherals and initializes code.

2.8 Data sampling through an ADC

In order to analyse an analog signal from the physical world in the digital world of a microcontroller the signal must be sampled and converted. This is done by an ADC which samples the analog continuous signal and outputs a digital, discrete-time signal that can be processed, see Figure 2.9. The resolution of the sampled signal from an ADC depends on how many binary bits are used during sampling, the bit length. The more bits the ADC uses for sampling the higher the resolution is after conversion. However, more bits in sampling also means more bits to process in conversion, which leads to a longer conversion time. Therefore, it might not always be better to use the highest resolution possible at all times, but rather as few as needed for the purpose. Another reason for this is that as the binary steps are smaller of a higher resolution ADC they can represent the analog signal in a better way, but this also makes the converted signal more prone to include noise [18].

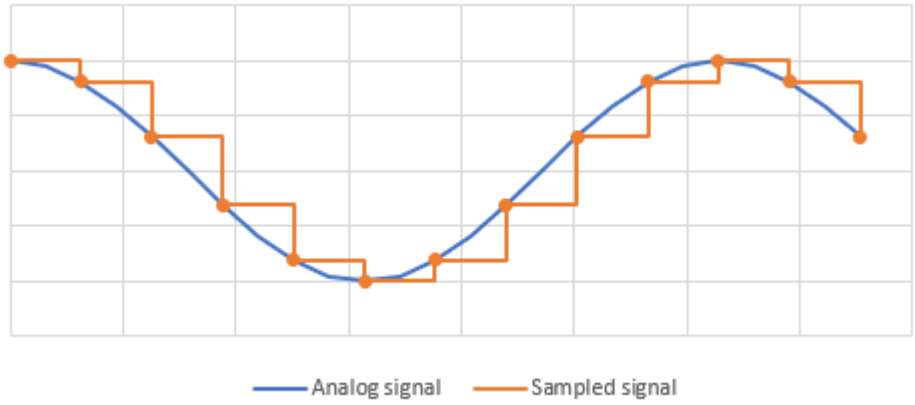

Figure 2.9: A continuous, analog signal and the sampled, discrete signal.

2.8.1 Aliasing

Aliasing is crucial to avoid as it means a high frequency signal can be interpreted as a low frequency signal if not sampled at a high enough rate [19]. When sampling a signal it is essential to consider the Nyquist-theorem. The theorem states that the sampling bandwidth must be at least twice the bandwidth of the signal in order to avoid aliasing. In other words, one must sample at least twice per period. Albeit, when it comes to recreating a continuous signal in the discrete time domain the more samples per period the better.

2.8.2 Direct memory access

In the usual case, when peripheral components of a microcomputer interact with each other the information is sent through and coordinated by the CPU. For low speed applications, this works fine, but in the case where an ADC samples at several hundred kilohertz the procedure is too slow and the CPU can't keep up the pace. Unless the CPU is quick and powerful, which is usually not the case for embedded systems. This problem can be solved by using a microcomputer that has direct memory access, DMA. DMA allows peripherals to send information to the memory without passing it through the CPU [20].

3 Electronic design

This section presents the first phase of the project where ultrasonic transducers were analysed. The aim of this phase is to produce ultrasonic waves by developing the circuits for both the transmitting and receiving transducer, recognizing the characteristics and limitations of the ultrasound.

This thesis work was carried out at Axis Communications AB. The company gave access to their electronics laboratory equipped with both tools and various components in terms of resistors, capacitors and alike. Below in Table 3.1 are the tools used in the development of hardware.

Table 3.1: The equipment and model used in the project.

Equipment	**Model**
Oscilloscope	Teledyne lecroy HDO6104B
Power supply	CPX400DP
Function Generator	SDG 1062X
Soldering stations	
Multimeter	Fluke 179
Thermocouple data logger	TC-08

3.1 Choice of transducer

First, the market was scanned for ultrasonic transducers to use in the prototype. The process commenced by identifying potential transducers suitable for easy integration and prototype building. DigiKey, an online distributor of electronic components, served as the primary resource for this search. A diverse array of ultrasonic transducers was found within their catalog. The transducers found on the market exhibited considerable diversity in terms of size, frequency range, operational temperature, and cost. The piezoelectric transducer turned out to be the most dominant technology.

The available piezoelectric ultrasonic transducers encompassed a spectrum ranging from disk sensors to encapsulated variants equipped with inter-integrated circuits. Prices spanned from 5 to 1000 SEK, reflecting the diverse functionalities and features offered by different models. To align with the project's

objectives of developing a prototype followed by potential integration into a system, the search was limited to individual transducers rather than complex integrated modules. Moreover, the search was restricted to pin-hole mounted components. Pin-hole mounted components facilitate practical integration and aim to expedite the assembly and testing phases, thus optimising the efficiency of the initial phase of prototype development. Surface mounted components are deemed to be unfit for prototype development as the risk of damaging the components is higher due to the short distance from the hot soldering iron to the sensitive part of the component.

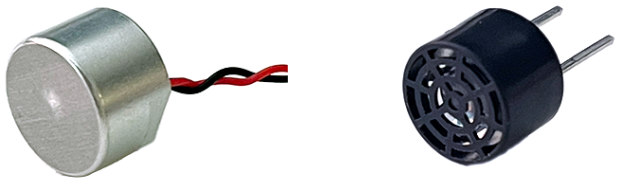

Figure 3.1: Closed top CUSA-TR50-05-2000-W68 (left) and open top Murata MA40S4S (right).

From scanning the market, only a few models met the goals of potential ultrasonic transducers. Referring to section 2.2, both the resolution and the Field of view (FoV) are depend on the frequency. Consequently, the price of the transducers on the market is also affected by the frequency. Keeping both the price and accuracy factors in mind, the decision was made to order the CUSA-TR60-06-2200-W68 to test out the performance of ultrasonic waves. The Cusa transducer operates at a frequency of 48 kHz, has a relatively broad beam angle of 120° in x- direction, and has an operating temperature range of -40 to 85° [21]. This transducer operates as a transceiver, both a transmitter and receiver.

The Cusa transducer operates at a high voltage, tolerating up to 150 V Peak to peak (p-p). The transmitter was first tested together with a power supply which offered a higher voltage supply through a transistor without success. The requirement of an impedance matching transistor showed out to be crucial in order to allow for large extraction of voltage through the transducer due to its capacitive behaviour. Considering both increased cost and size associated with implementing a transistor drive, a decision was made to revisit the market in search of alternative transducers that operate at lower voltages. By adhering to the constraints of operating temperature, the available options

were limited. However, the MA40S4S, an ultrasonic sensor manufactured by Murata Electronics, emerged as a promising transducer candidate.

The Murata transducer is of open-top and is therefore more sensitive and has a p-p driver voltage of 20 V [22]. However, the transducer did not meet the demand of a broader beam angle and had a somewhat lower frequency than the Cusa transducer, of 40 kHz. Additonally, the Murata transducer is not of dual use with the transmitter and receiver having different characteristics. The transmitters are optimised to generate maximum sound pressure at 40 kHz, whereas receivers are tailored for optimal sensitivity at the same frequency. The transducer has an outer diameter of 10 mm and directivity of 80° [23]. More detailed graphs over the Murata transducer characteristics are available in Appendix B. Despite the transmitter and receiver modules serving different functions, the difference were deemed negligible for this application. Consequently, the decision was made to procure the transducer to function as both transmitter and receiver, given the status as the sole available option at the time. Using a set of different sensors could potentially improve the accuracy, but was not investigated in this project.

3.2 Development of circuits

The ultrasound transmission circuits were initially prototyped using breadboards and standard passive electrical components sourced from the electrical test lab at Axis Communications. This initial phase allowed for rapid experimentation and iteration, enabling the exploration of various circuit designs and configurations. Subsequently, the circuit designs were simulated in LTspice, a circuit simulation software. Following successful validation, the finalized circuit configurations were transferred onto veroboards through soldering, aimed at minimizing noise interference and ensuring optimal performance.

3.2.1 Driver circuit

To transmit ultrasonic waves, the transducer needed to be driven with pulses at its resonance frequency. Initially, a direct driver was constructed to drive the transducer with a 3.3 V signal, directly from the MCU. However, due to disturbances proportional to the ringing time, the emitted sound pressure needed to be increased. The emitted sound pressure level is voltage dependent and therefore a MAX232 IC was introduced. The MAX232 served as a voltage amplifier, providing the maximum driving voltage of 20 Vp-p solely from the 5 V source supply.

The MAX232 needs to be surrounded with five capacitors for doubling and in-

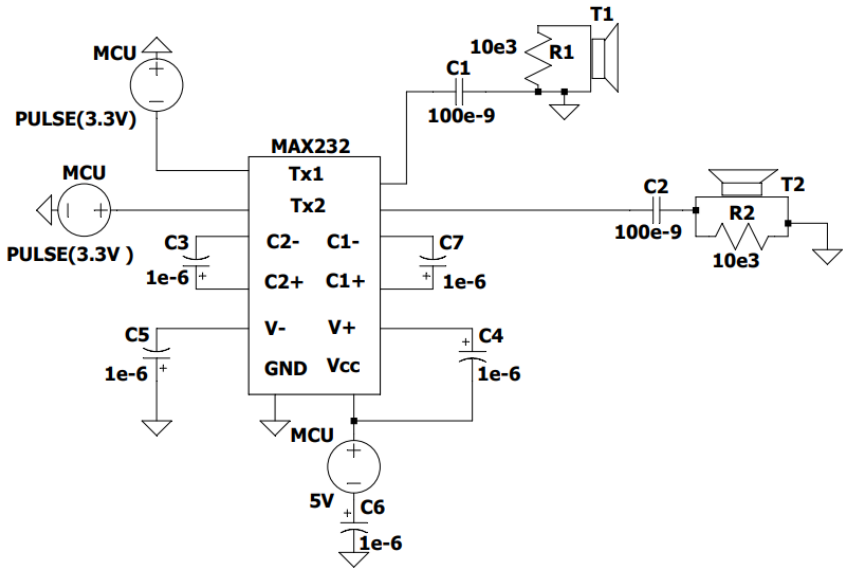

Figure 3.2: Transmitter circuit direct drive for two transmitters. Pulses generated with PWM output of the MCU.

verting the input voltage. Despite following the recommended circuit retrieved from the data sheet, the breadboard construction did not perform as desired [15]. Presumably, the disturbances were due to EMI. The circuit worked as expected after it was soldered onto a veroboard, eliminating long cables acting as antennas. Additionally, a DC blocking capacitor and a parallel resistor were put before the transducers, shifting the default voltage from 10 V to 0 V and eliminating overshoots. The final transmitting circuit diagram is provided in Figure 3.2.

3.2.2 Pulse configuration of sonic burst

The sound pressure energy emitted is not only dependent on the driver voltage, but also dependent of the number of pulses. Therefore, the number of sonic bursts needed to be tailored to the specific requirements of the project. The STM32 Nucleo-64 development board was used for generating pulses. The choice of board is further discussed in section 4.1. For transmitting ultrasound the MCU utilized the advanced timer TIM1, which was configured as an output in One-Pulse mode, a Pulse-width modulation (PWM) setting with only one pulse instead of a continuous signal. The clock settings were set to achieve PWM output, at 40 kHz with a 50% duty cycle. Together with Repetition-Counter, the number of pulses could be repeated to the desired number of times.

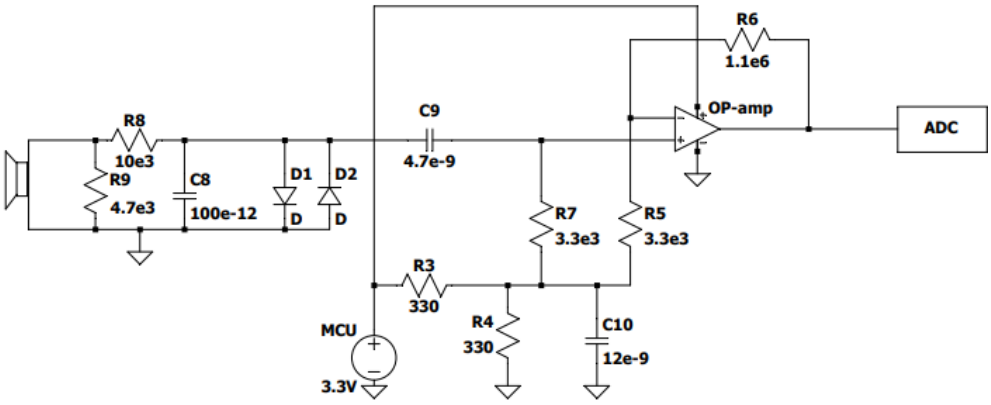

Figure 3.3: The circuit used to amplify and filter the received signal.

3.2.3 Receiver circuit

Without any modification, the receiving ultrasonic wave was of low amplitude and therefore needed to be amplified. With inspiration from a project on a ultrasonic position system for electric road [24], a receiver circuit was constructed. Due to disturbances, it is essential to amplify and filter the signal close to the receiving transducer before the signal proceeds through any long cables. The receiving circuit consisted of a low pass filter, a pair of voltage limiting diodes, a DC blocking capacitor followed by a non-inverted operational amplifier. The final receiving circuit diagram is provided in Figure 3.3.

From the MAX232 IC, both a negative and a positive voltage of 10 V is created. This voltage was at first intended to be used as supply voltage to a series of operational amplifiers, resulting in a high gain and a low pass filter of higher order. However, the Nucleo board only allows for voltage in the interval from 0 to 3.3 V. A biased voltage of 1.65 was therefore constructed with a voltage divider and summed to the ultrasonic signal restricting the signal to oscillate around the biased DC offset.

3.3 Performance tests

In this section, the performance of the ultrasound transducer was investigated. The performance of the Murata ultrasonic transducer was tested together with a simple direct driver and with a maximum voltage supply driver represented in Section 3.2.

3.3.1 Test: Pulse dependence

By alternating the repetition counter on the MCU, the dependence of the sound energy transmitted could be observed on the amplitude of the receiving wave. The cycles of sonic burst were tested in the range from 1 to 8 pulses, with the receiver being positioned at both small and big angles of divergence. The transducers were orientated towards the center of a circle with a radius of 120 mm. The set up is illustrated in Figure 3.4.

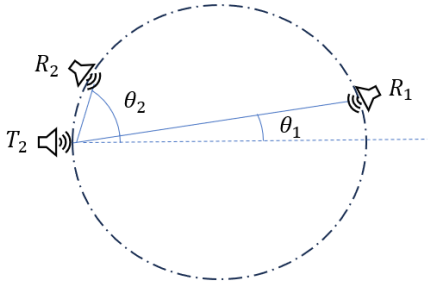

Figure 3.4: The test setup for distance reading with one transmitter T_2 and two receiver, R_1 and R_2, with two different angles of divergence, replicating the scenario in the proposed concept.

In Figure 3.5, the received ultrasonic wave is observed for one, respective eight, pulses. The yellow channel represents the 3.3 V PWM output directly from the Nucleo board and the blue channel is the receiving ultrasound after being filtered and amplified by the receiver circuit. As the number of pulses increased, so did the amplitude of the received signal.

Some coupling, interaction between the transmitted pulse and received signal, can be observed in Figure 3.5. This unwanted disturbance, also known as cross-talk, is most likely caused by the remaining energy from the direct wave or small movements in the air. The coupling interferes with the received wave and affects the accuracy for short distances. Good accuracy is desired for the full range to get a precise angle measurement for the concept. Therefore, there is a desire to keep the sonic burst to just a few pulses, but still send a wave strong enough that is detectable at full range.

3.3.2 Test: Voltage dependence

The emitted sound pressure level is also dependent on the driver voltage. By introducing the MAX232 circuit the transducers could be driven to their maximum rated voltage. The received signal was analyzed. In Figure 3.6 the green channel represents the PWM voltage. The blue channel is the voltage applied

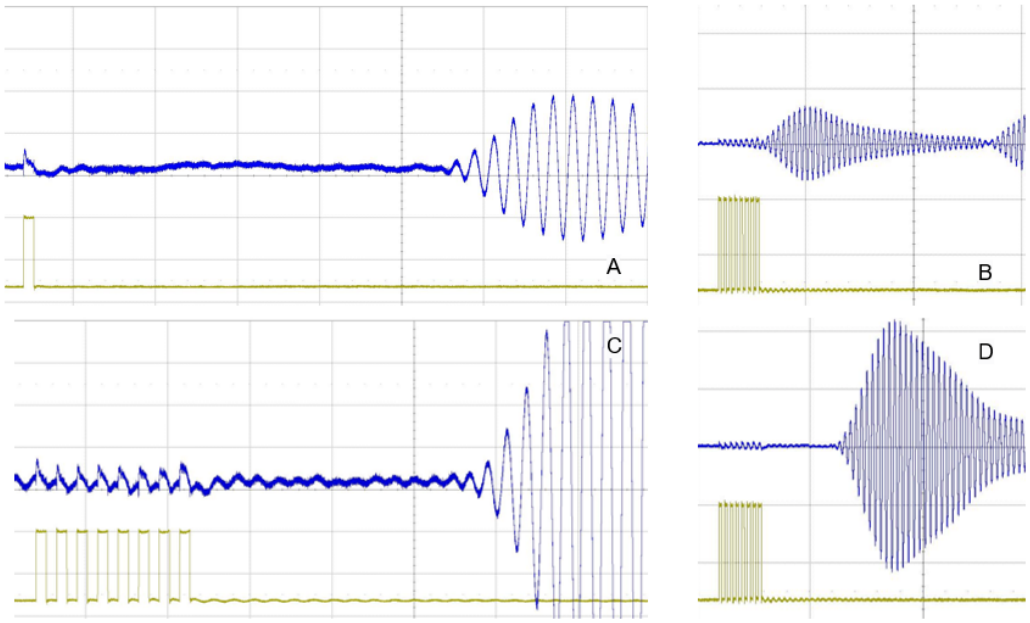

Figure 3.5: Receiving wave is dependent on the number of pulses and the beam angle. Figure A and C respectively B and D has the same scaling. A: 1 pulse at θ_1. B: 8 pulse at θ_2. C: 8 pulses at θ_1. D: 8 pulses at θ_1 again.

on the transmitter which is pushed to its maximum peak to peak, shifted to 0 / -20 V through the DC blocker, and then starts to oscillate in its resonant frequency by the remaining energy from the burst. The yellow channel represents the receiver signal, and has a detectable response for shorter distances compared to the 3.3 V pulses.

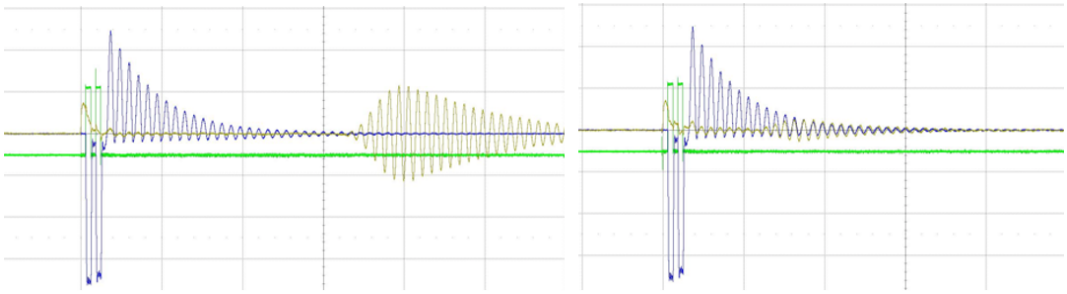

Figure 3.6: Performance from two pulses and maximum voltage p-p V, at θ_1 (left) and θ_2 (right).

In Figure 3.7, an enlarged image of the pulses generated from the MCU the disturbance due to the triggering, and the resonance oscillations is shown. It is noticeable that the receiver circuit takes up noise from when the trigger is set, which is caused by a pin set to high on the Nucleo board. The receiver

then oscillates as a response to the cross-talk. This ringing attenuates after about 300 µs and then the signal can be considered as solely noise. By the idea of superposition, this constant oscillation could be subtracted and even a shorter distance could be detected with higher accuracy. This idea was set aside for further investigation until the overall performance was tested.

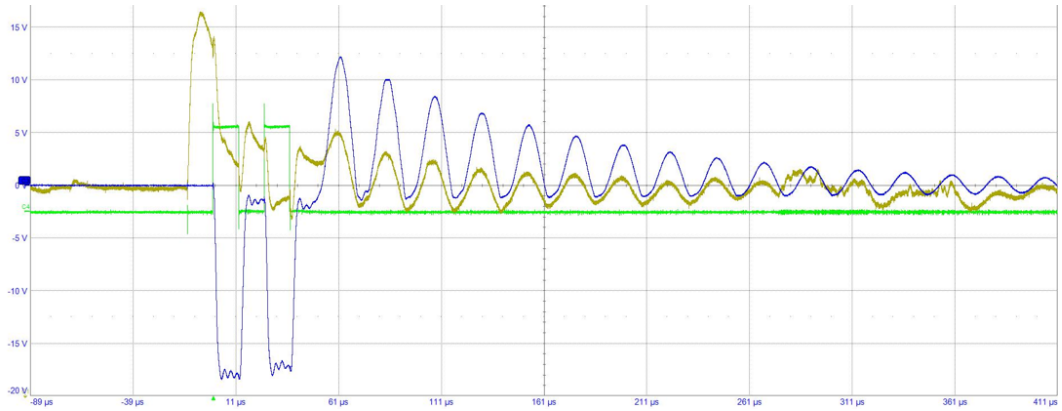

Figure 3.7: The pulses and oscillation at resonance frequency for both transmitter and receiver.

3.3.3 Test: Attenuation

During the previous tests, mainly the first sound pressure waves were observed. However, due to echo and reflection, the second and third waves needed to be taken into account. By introducing the walls made out of different materials, the effects from reflection and sound absolution were investigated. The three materials considered were metal, cardboard, and plastic foam, see figure 3.8.

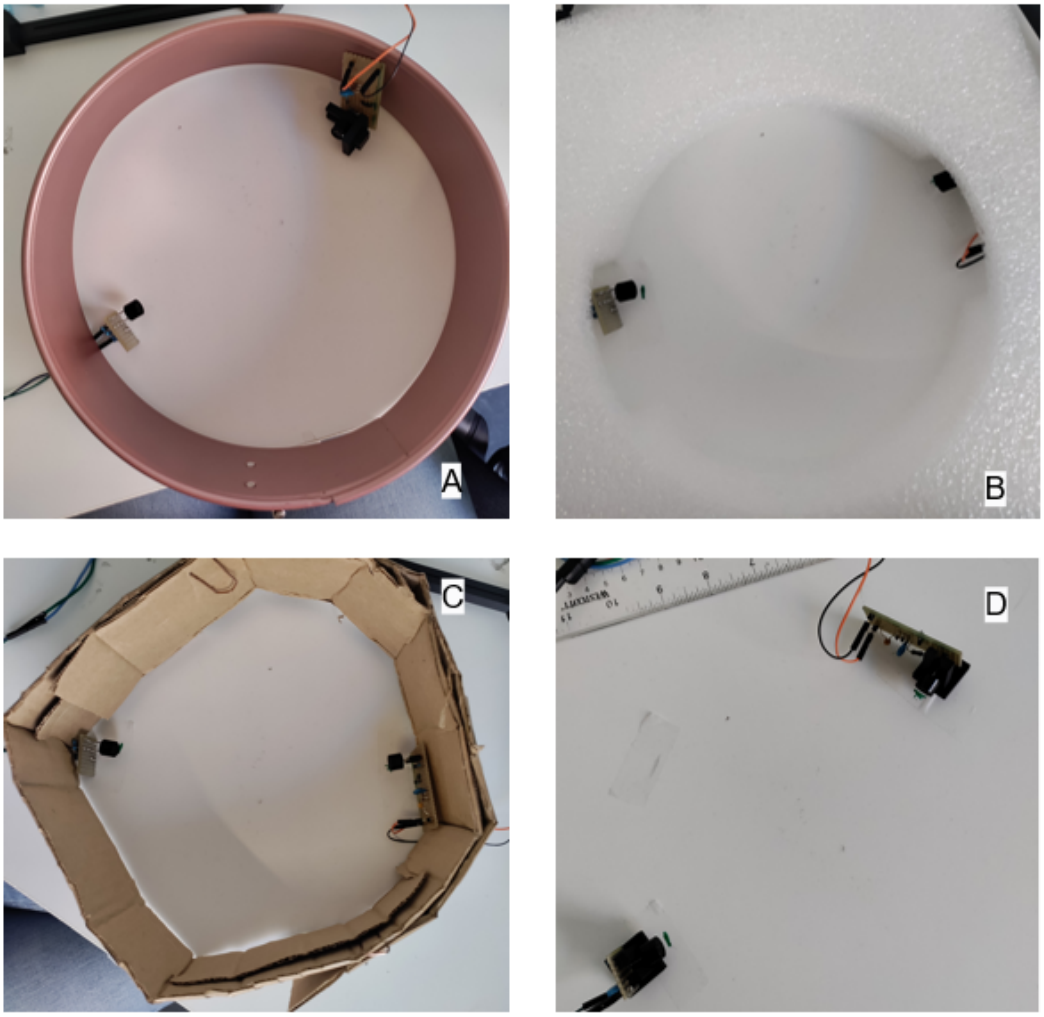

Figure 3.8: A: Metallic baking tin, B: plastic foam used for emballage in packaging and C: rolled cardboard. D: the same set up without any surrounding walls.

Figure 3.9 shows how the material of the walls had an impact on the signal. With metallic walls, the signal had a long attenuation time, up to 10 ms before the signal could be considered as just noise. In addition, there was a large disturbance due to the direct wave. For cardboard walls, the impact from the cross-talk was of less amplitude and the total ringing time was reduced to 5 ms. The results showed that the plastic foam had the similar receiver response as with no walls at all. For plastic walls and without walls, the attenuation time were 2.5 and 3.5 ms, respectively.

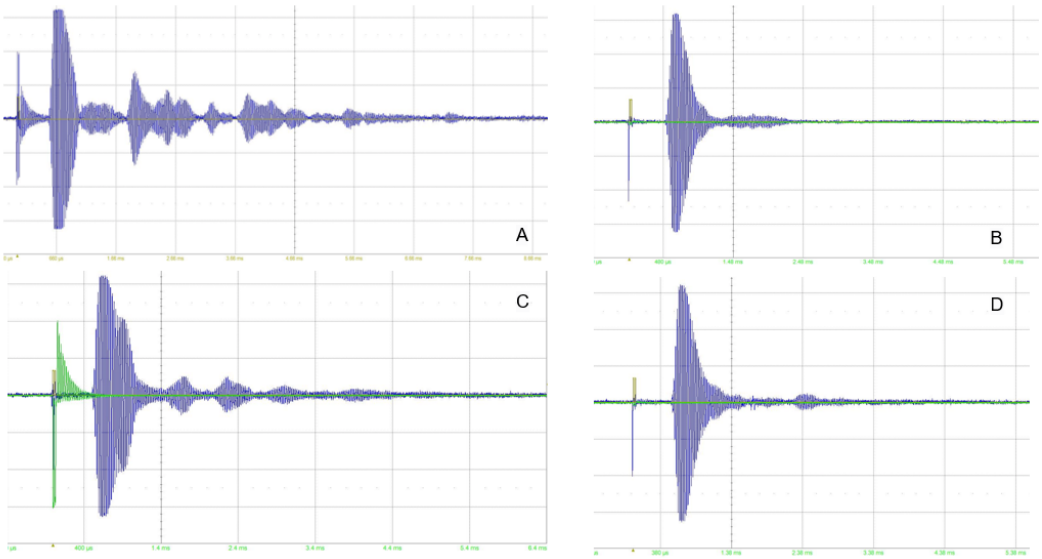

Figure 3.9: A: receiver response with walls made out of metallic, B: plastic foam, C: cardboard. D: The received signal without any surrounding walls.

The test shows that isolating the walls with proper sound-absorbing material can reduce the attenuation time. The echoing for the plastic foam was similar to the test without walls. This means that an attenuation time of 3.5 ms needs to be taken into consideration in order to not let the next transmitted ultrasonic pulse interfere with the remaining echo.

3.4 Conclusion

Despite that the Murata transducer has a directivity of 80°, the test showed that the FoV still covers a larger angle required for the concept. Two pulses with maximum driver voltage proved to be the best combination to detect ultrasound for both big and small beam angles for the given range without significant disturbances from electromagnetic coupling.

4 Software, signal processing and calibration

This chapter focuses on the development of the software and signal processing performed on the MCU. Furthermore, the chapter explains the methods used to calibrate parameters for optimal performance and accuracy.

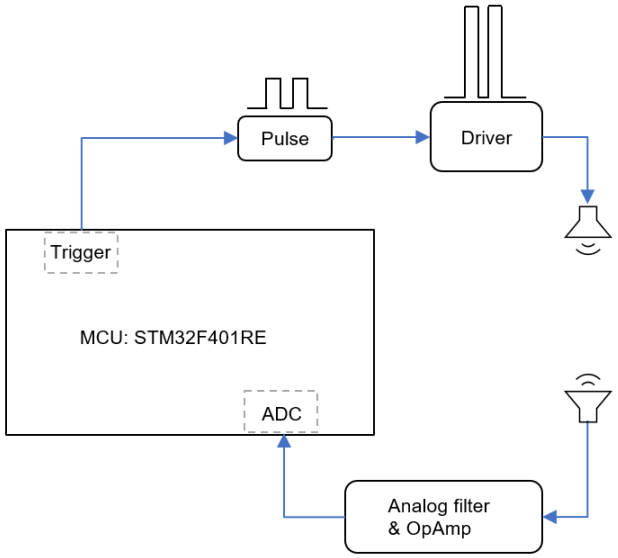

Figure 4.1: A visualisation of how the signal travels through the system in principle.

4.1 Choice of MCU and software environment

Before developing the software, the appropriate hardware must be selected to run it. In the initial stage of the project, some criteria were set for what features the development board must attain. The vital features were a clock speed faster than 50 MHz, ADC with DMA and the FPU.

These criteria reduced the number of boards to choose from. One of the boards that fulfilled the criteria was the board mentioned in section 2.7. What distinguished this board from the other alternatives was its availability in stock at the company. The availability led to a short start up, as the shipment was immediate, and also a reduction of costs in the initial phase.

A benefit of choosing the boards produced by ST Microelectronics is that they also provide an IDE, STM32CubeMX, specifically made for programming their boards. The IDE allows easy configuration of the different pins on the development board and code generation for the same purpose. The code that is generated by STM32CubeMX is in the programming language C and therefore constituted the language used in this project.

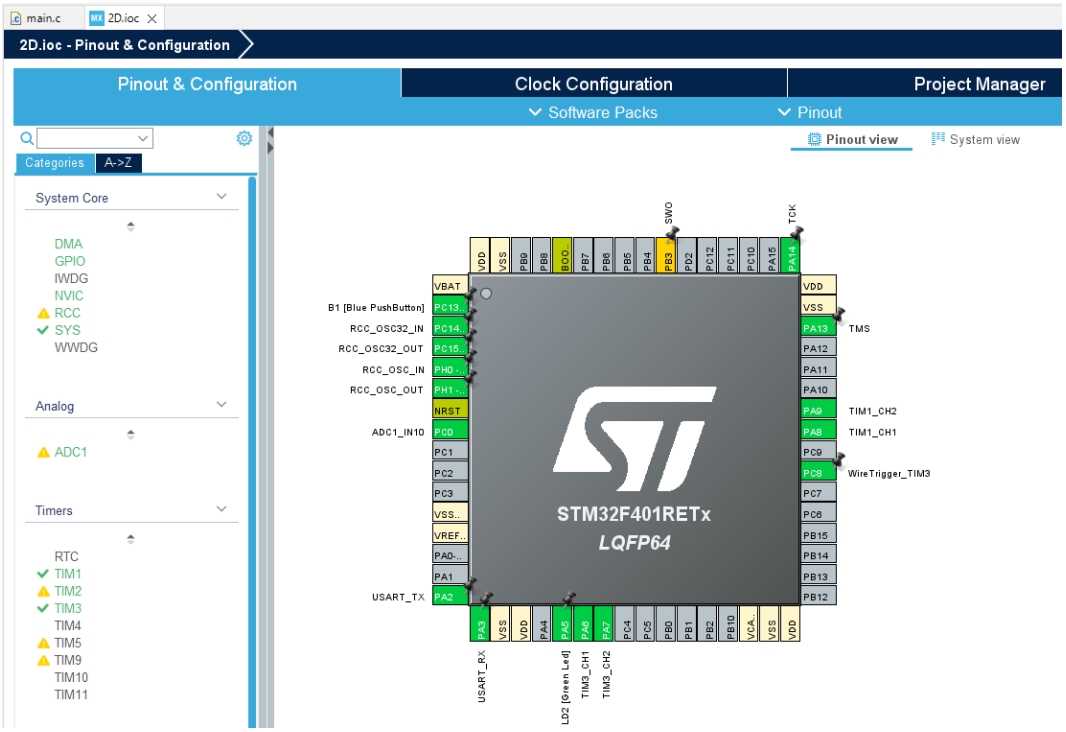

Figure 4.2: Screenshot of the view in STM32CubeMX and the pinout configuration.

4.2 Sampling of analog signal

To process the signal, the receiving ultrasound was collected with an ADC which stored the data in the memory using the DMA feature. To confirm that the ADC sampled at the desired frequency and that the sample time was long enough to get an accurate measurement, the sampled data was sent via UART to the terminal emulator PuTTY on a computer and visualised in MS Excel. For this verification step, the signal to be sampled was transmitted from a function generator and in the first stage the signal was a 40 kHz square wave. This was chosen as it was thought to be an easy waveform to detect any deviation from. The sampled wave was compared to what the generator was set to and what was seen on the oscilloscope. A sampling time that was

too short was identified from observing a non-square waveform. The reason for this is that the capacitors weren't charged long enough, thus leading to incorrect sampling. Here, it must be clarified that the sampling frequency or the sampling period, is not equal to the sampling time. A sample period consists of two stages. The first one is the sampling time, where the capacitors are charged with electrical energy and the second one is the conversion time of the sampled data. As mentioned section 2.8, a higher resolution leads to a longer conversion time as it is more bits to process. When the sampled square wave looked as expected the settings of the ADC were tested against two other waveforms, sinusoidal and triangular. The default value of resolution in the IDE was 12 bits. As the ADC worked up to expectations this was not changed, but left to be adjusted later on if needed.

As described in section 2.8.1 one must sample at least twice per period to avoid aliasing, but it is beneficial to sample even more often. Therefore, the sampling rate was chosen to be 480 kHz which resulted in 12 samples per period of the ultrasonic signal. As the ADC frequency is based on the clock speed of the MCU, the clock speed was changed to achieve the desired sampling frequency. Parallel to the setup of the ADC, the same thing had to be done for the DMA feature. Although, this could not be tested in the same way. If the data was captured, sent and when displayed on screen looked like the wave showed on the oscilloscope it was considered good enough. Lastly, the ADC was configured to start by the code after the pulses had been emitted. The buffer size of the ADC was trimmed to capture the ultrasonic waves for the maximum distance, but kept as short as possible to save processing time.

4.2.1 Calibration of data sampling

Despite setting the sampling frequency to 480 kHz, the actual frequency might differ from the programmed in any software implementation in embedded systems. Therefore, the sampled data was compared to the data captured on the oscilloscope. By identifying peaks in the oscillation, values were matched with the time stamp for the same peak given by the oscilloscope. The same test was performed a couple of times, on different sets of ultrasonic waves, in order to verify the values. The result of the matching and the linear regression is represented in Figure 4.3. An average of the test results is presented in Equation 4.1

$$y = \frac{x}{0.48315} + 23.33. \tag{4.1}$$

The proportional gain in Equation 4.1 represents the time passed between samples in microseconds. The inverse of the gain is the actual sample rate.

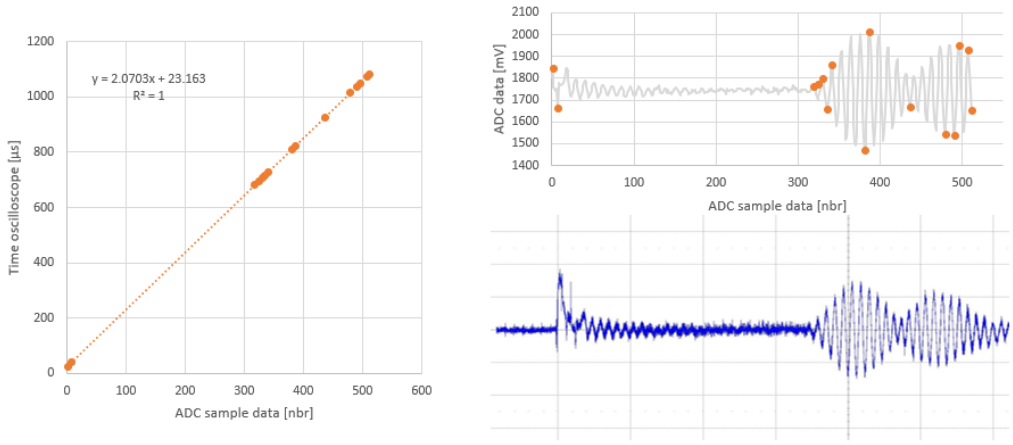

Figure 4.3: The linear regression of sampled data to the left. The sampled signal and the point matched with the corresponding diagram captured on the oscilloscope to the right.

The average value resulted in a sample frequency of $f_{sample} = 483.2$ kHz. As the clock speed of the MCU is based upon a crystal, with a given resonance frequency, not all clock speeds can be achieved as a prescaler must be used to get any other frequency than the crystal's. This allows for a fairly accurate clock speed, but for some occasions, not the exact one desired. The error follows onto the ADC as its frequency is based on the frequency of the MCU. The frequency is expressed in MHz. The constant in the Equation 4.1, represents the time elapsed from when the transmitter is triggered to when the ADC starts sampling, is expressed in microseconds. The average startup time delay for the ADC proves to be $t_{DelayADC} = 23.33$ µs. The delay indicates a dead zone about 8 mm where a first received signal can't be sampled. The actual sampling frequency compared to the programmed one, had an error of 0.66%. Although it is a small error it has a significant impact on the length measurement, especially as that is based on the sampling rate.

4.3 Distance reading

To get a distance measurement the first step was to gather the ToF. This information is embedded in the sampled received signal. The sample frequency and the velocity are known parameters, hence a time delay can be calculated.

The ToF was calculated by performing cross-correlation on the sampled signal and a reference signal. As written in section 3.3.1, both the shape and the amplitude of the SPL and received signal vary with the receiver's loca-

tion. From trials, it was noticed that the cross-correlation output was not trustworthy when the signal had more than one bulge, depicted in Figure 4.3. This is because the cross correlation method is dependent on the shape of two signals being correlated. To counter this problem a threshold was introduced which the signal needed to surpass. To be certain that the threshold was not triggered by noise, a function was introduced which checked that the threshold was exceeded for six consecutive periods, ensuring continuous oscillations of higher amplitude. After these periods the sampled signal was cut and set to zero.

The resolution of the calculation is determined by the sample frequency and temperature. With the given sample rate the resolution is, in theory, about 0.7 mm in room temperature. From the correlation method, the distance is calculated accordingly with the following equation:

$$t_{ToF} = \frac{X_{corr}}{f_{sample}} + t_{DelayADC}, \tag{4.2}$$

where X_{corr} is the correlation peak obtained through cross-correlation, f_{sample} is the sampling frequency and $t_{DelayADC}$ is the startup time of the ADC. X_{corr} is affected by the speed of sound, which in turn is dependant on the temperature.

4.3.1 Distance accuracy

The foundation of the angle measurement is a good distance reading due to the fact that the angular reading simply consists of two consecutive distance measurements followed by calculations, which are explained in section 2.1. Therefore, the distance accuracy has to be as good as possible to the best angle accuracy.

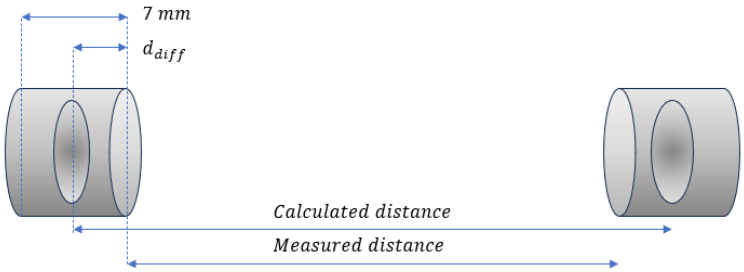

Figure 4.4: The dimensions of the Murata transducer and the illustration of the calculated and measured distances.

To evaluate the correlation method, a linear accuracy test was performed. The test was executed by placing two transducers facing each other, along a

ruler on the table. The distance between the two fronts of the transducers was alternated from 60 mm up to 300 mm, and this composed the measured distance that the algorithm was compared against. Before the test, the ambient temperature was read using a thermocouple data logger and updated manually in the code to calculate the speed of sound. Each measurement was performed ten times, and the mean value of each set of measurements was used to evaluate the distance reading, see the result in Figure 4.5.

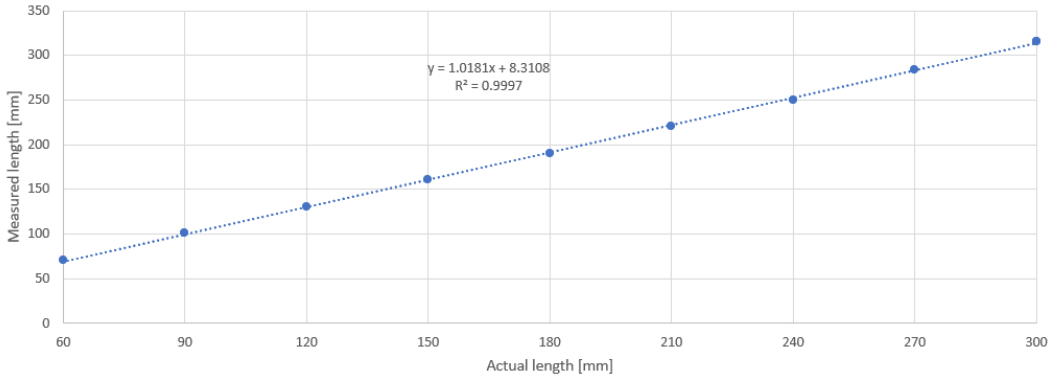

Figure 4.5: The calculated length as a function of the length between the front face of the transducers.

From Figure 4.5, the linear regression indicates that the calculated distance is not linearly proportional to the measured one, despite that the temperature was updated before the measurements and the sampling frequency had been calibrated. The constant of the linear regression indicates a difference between the front face of the transducer and the actual piezoelectric element inside the case about $d_{diff} = 4$ mm, see Figure 4.4. Taking the distance difference into account, the distance measurement was calibrated.

Notably, the gain indicates a measurement error as it is not equal to one. With a perfectly calibrated frequency rate and an updated velocity, the gain ought to be one. During the calibration, transducers were facing each other alongside a ruler. This way of testing should be a proper way to test the linear accuracy. The one aspect of the measuring method which is negative is that it was done by an ocular reading of the ruler and placing the transducer accordingly. The lack of accuracy inherent to an ocular reading and manual placement of the sensor constitutes a source of error that needs to be considered. It is estimated that the human error factor could in this case place each transducer within 1 mm of the desired location. This factor guarantees a deviation from the total length of ± 1 mm. Besides the human factor in the measurement, small temperature variations may have affected distance reading. Finally, the sampling frequency has an impact on the distance reading accuracy as a higher sampling frequency leads to a shorter distance the sound wave can travel between samples. Therefore, the higher the sampling frequency, the better the accuracy.

5 Performance tests

This chapter presents the testing methods that were performed to evaluate the prototype. By testing different aspects of the prototype, the aim was to identify any potential issues and gather valuable feedback for further refinement of the concept.

5.1 Prototype development rig

For the sake of development, a prototype rig to mount the transducers on was created using Computer-aided design (CAD)-software, see Figure 5.1. The rig was drawn to allow easy access to transducers, in case one must be swapped, and to be able to set to a wide range of angles, which had to be easily read with a protractor. This was achieved by creating a 1 mm wide groove along the centerline of the arms to be used as a reference for the protractor. The rig had two fixed arms with 90° between them and another arm which rotates around the center. At the end of each arm was an extruded square cut where the holder of a transducer was to be placed. The holder had a corresponding extruded square on the bottom and at the top, it had two pillars which the transducer's pins were to be placed between.

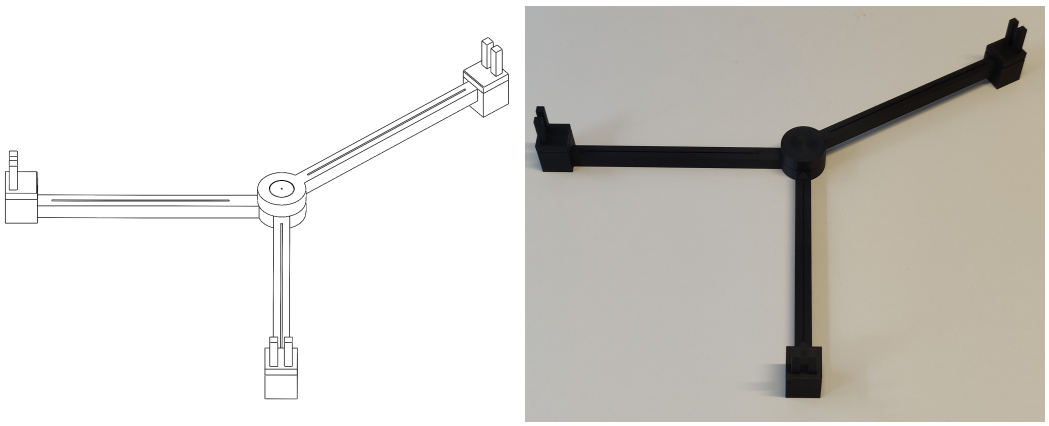

Figure 5.1: The prototype as a CAD-drawing (left) and what it looked like after 3D printing(right).

A benefit of purpose drawn prototype for this case is that the radius would be fixed throughout the testing. Simply the fact that the radius was known

from design removes a large uncertainty when calculating an angle as that parameter is of great importance. As this thesis aims to develop a proof of concept a delimitation was made here that not all angles around the circle could be measured. This simplified the drawing process and was expressed through the mechanical design of the rig.

5.2 Distance measurement with walls and roof

In section 3.3.3 it was investigated how walls of different materials affect the received sound wave. In this test, both walls and a roof made out of cardboard are introduced to investigate how much effect the reinforced oscillation has on the distance measurements. The wall was made as round as possible and of a diameter as close to the outer edge of the prototype rig as possible. The roof in this test where placed about 5 cm above the transducers. For this test, the transducers were positioned with a 90° and at 110° difference relative to each other.

5.3 Objects in flight path

The product specification requires that a position can be determined with obstacles placed between the transmitter and the receiver. Tests were performed to see the effect on the accuracy of various objects placed in the flight path of the wave. Such a scenario could happen if the cables within the electronics in the optical module end up in the plane where the ultrasonic wave travels. The robustness was tested by introducing a set of cables of various sizes in the ultrasonic flight path. The cables were placed directly in the line between the transmitter and receiver. The first objects to test were six separate cables with a diameter of 1 mm and both ends connected on a breadboard. Afterward, the test was repeated with three 2 mm loosely intertwined cables bundled up into a loose nest. These two cases are depicted in Figure 5.2.

5.4 Angular measurement

The algorithm used to determine the angular position is visualized by the chart in Figure 5.3. The block *Calculate angle* uses two distances, an X-distance and a Y-distance, each related to one transmitter, and calculates each possible position, referring to section 2.1. The algorithm then takes the two closest angles and presents the average of these as the position.

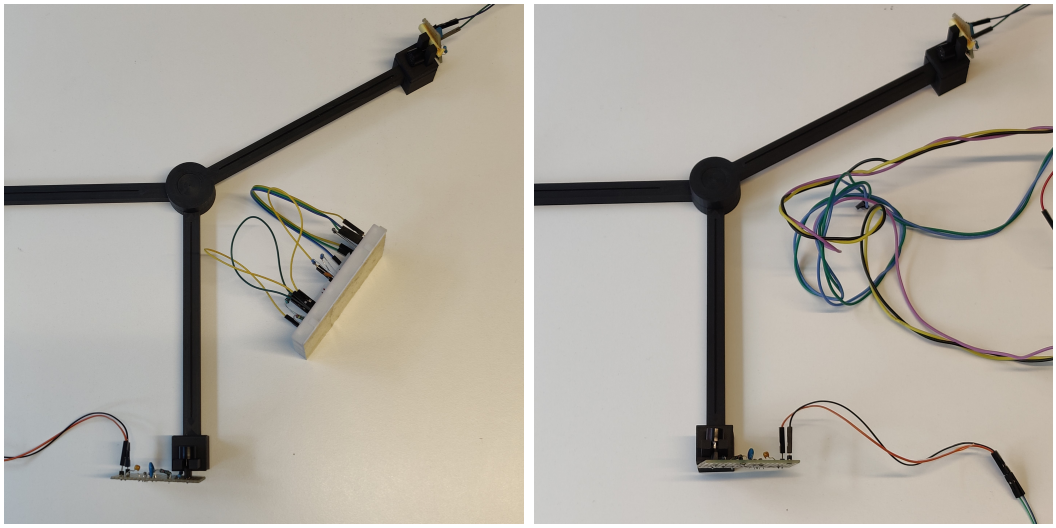

Figure 5.2: The figure show how small cables (left) and larger cables (right) were placed in the flight path.

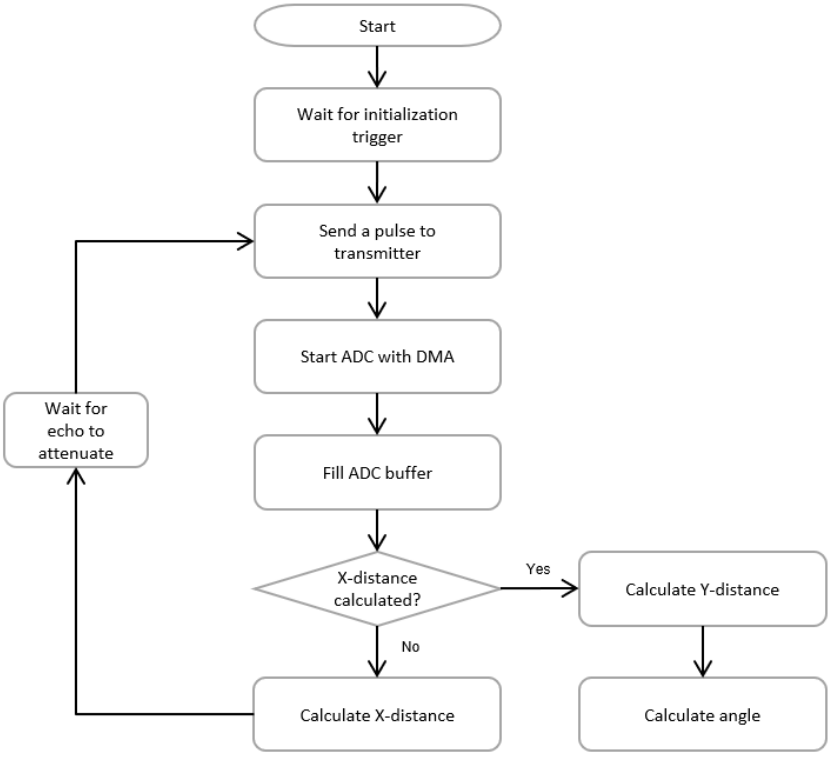

Figure 5.3: The flow chart visualises how the implemented algorithm of the system works.

5.4.1 Reduction of pulses

As described in section 3.4 the best performance was achieved by sending two pulses with maximum excitation voltage. In implementation, this worked well for one transmitter, but challenges occurred when the same was tried to be implemented for two transmitters. Instead, a test was done to see how well it would work with only one sonic burst. No significant differences where found when comparing the distance readings obtained with one pulse and two pulses. In line with the philosophy of development in this thesis, described in section 1.5, the number of pulses was reduced to one at this point and the development process continued.

5.4.2 Angle measuring method

The angular position was measured by placing a protractor at the center of the prototype rig and rotating the movable arm with the receiver on the end to the desired angle. The protractor's center point was aligned by sliding it against a block held against another arm, thus fixating it in one direction. The other direction was adjusted manually until the center point of the protractor aligned with the rig's center point, as seen in Figure 5.4. Before each test, the temperature was measured and updated in the code to account for changes in the speed of sound.

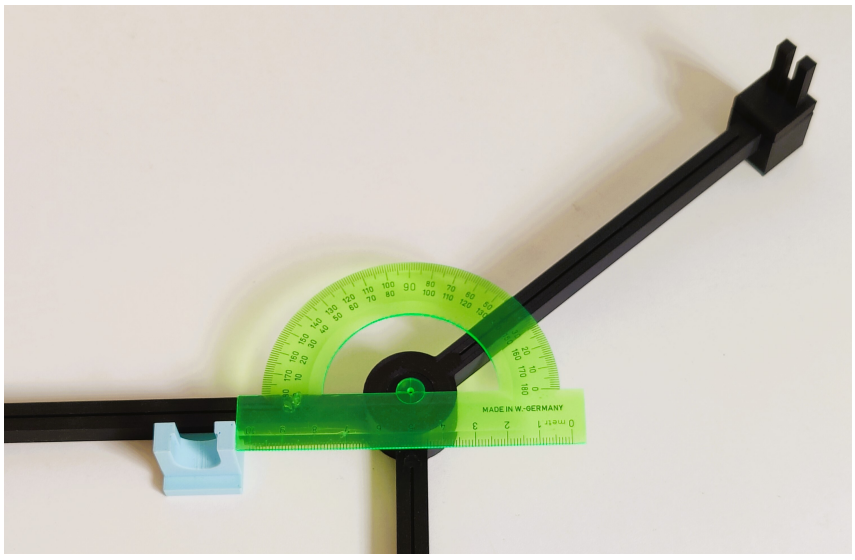

Figure 5.4: The figure show how the protractor was placed and fix it in one direction against the blue block.

5.5 Evaluation of input variables

Except for the temperature, the only variable in the algorithm is the length of the radius upon which the transducer is mounted. From calibrating the distance reading, d_{diff} was estimated. Due to the human errors in the estimations, it was investigated what effect the parameter had on the measurement. This was done by taking the same set of distance readings but basing the position calculations on a slightly altered radius.

6 Results and Discussion

This chapter presents the results from the tests described in chapter 5. The result is followed by an evaluation and discussion of the knowledge acquired from each test.

For each test, a set of 10 measurements was evaluated and the spread of the measurements is represented in box plots. Noticeably, there were variations for some of the readings indicating that the concept was not perfectly robust. The box represents the interquartile range, which shows the middle 50% of the readings. Whiskers represent the other 50% of the readings. Additionally, outliers might occur and are represented by a dot in the plots. The outliers show that the distance reading was sensitive and therefore the evaluation of the results is based on the mean value, indicated by a cross.

6.1 Distance measurement with wall and roof

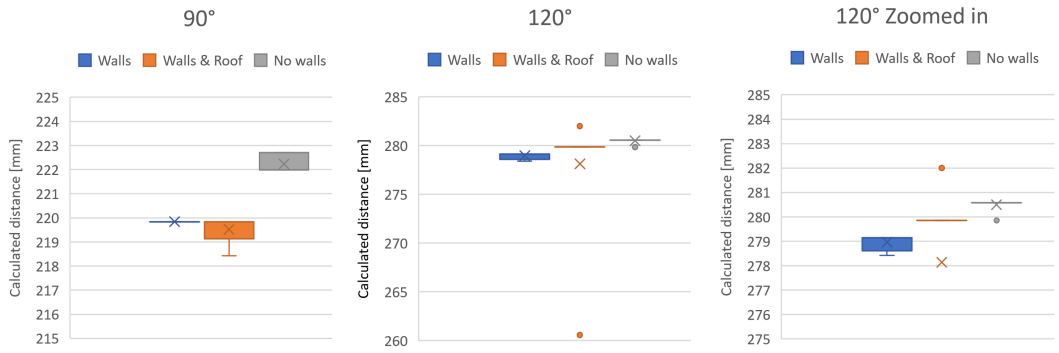

Figure 6.1: The figure illustrates the effect of enclosing the prototype rig with walls, respective walls and a roof for two different angles, each with a radius of 160 mm. The subfigure on the right excludes an outlier and provides a zoomed-in view of the remaining data for better visualization.

From Figure 6.1 the impact of introducing walls and roof is evaluated. A relatively large distance was chosen to let the direct wave ringing decay. Despite that, there is a noticeable decrease in distance reading accuracy when surrounding walls are added. The distance reading is reduced even more when

the roof is added. Most likely, the decrease in distance is due to that the surrounding environment, made out of cardboard, reflects ultrasonic waves. The remaining energy amplifies the small oscillation and is superimposed with the ultrasonic wave.

During testing a large effort was put into not disturbing the setup of the transducers, but inevitably some contact was made when introducing walls in the test. This is regarded as a source of error. Nevertheless, the differences between them were less than 5 mm as seen in figure 6.1. A relatively small error, but still large enough to have an effect when measuring the angle. This proves the importance of sound absorbing insulation around the measuring field.

6.2 Foreign objects in flight path

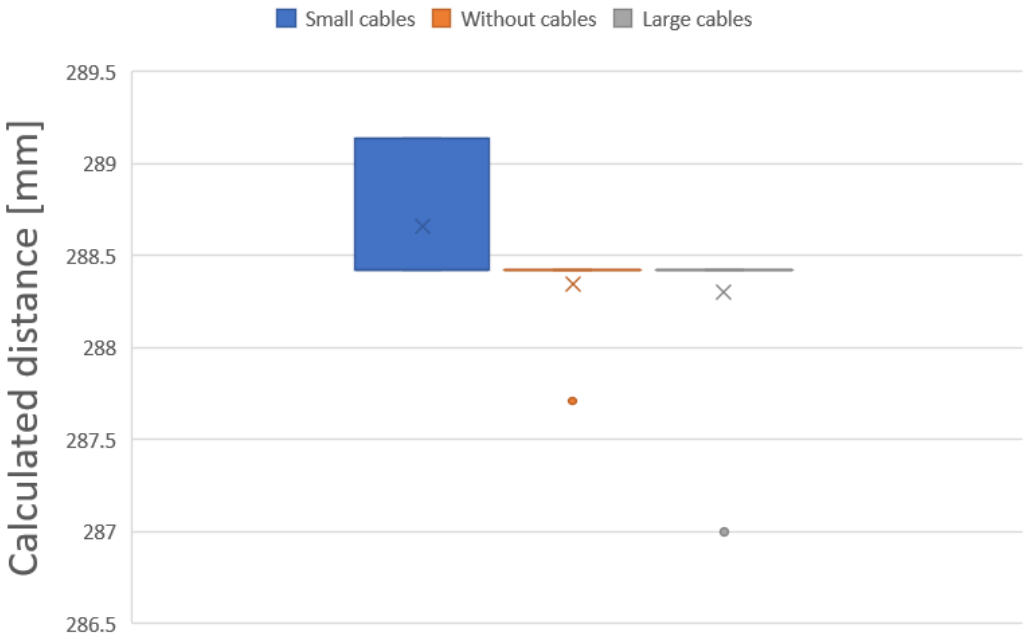

Figure 6.2: The figure shows the robustness against foreign objects placed in the flight path.

A scenario in which some internal component or cable has come loose is the most probable scenario that would alter the space where the ultrasound travels. As seen in the result, no or very little difference in accuracy can be detected when foreign objects are in the flight path. These are very favorable results for the concept developed in this thesis. From this, it can be concluded that it is not always necessary to repair or replace a camera if something has come

loose internally, as the position calibration still operates as usual.

6.3 Angular accuracy

In figure Figure 6.3 the distance measurements of an angular reading are presented. What can be noticed is that the mean of each box follows an expected trend around the circle. The two transducers have a similar shape of the function and they appear to be shifted 90° from each other, just like in the prototype.

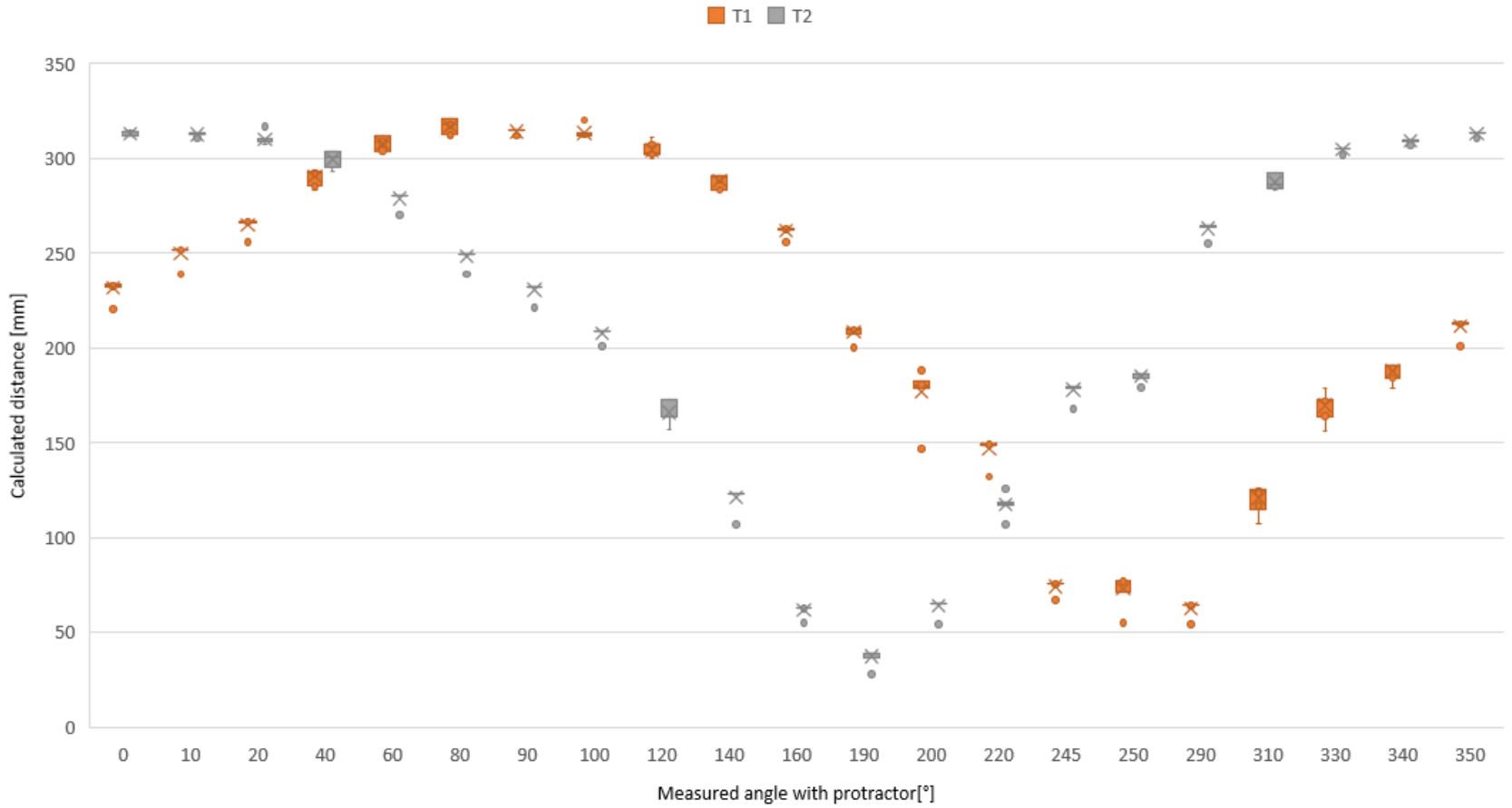

Figure 6.3: The distance reading for transducer T1, respectively T2. Notice that the angle scale is not evenly distributed due to the "dead zones" at 180° and 270 °.

Figure 6.4 represents the position deviation. This result is the culmination of the thesis work. However, the result can not be considered precise with a total spread of ±8°. Moreover, the position deviation does not fulfill the prototype's requirements by a rather large error. Noticeably, there is a trend for better accuracy in the first and third quadrants, with a position deviation of ±4°. However, the second and fourth quadrants are not as accurate. This trend follows a line of 45° in the coordinate system. The reason for this is suspected to be a consequence of the error in distance measurement. In quadrants one and three, the distances to the two transmitters are about the same length, whereas in quadrants two and four, one distance is significantly shorter than the other. The errors cancel each other out where the distances are similar, resulting in better accuracy. However, this is not the case for quadrants two and four.

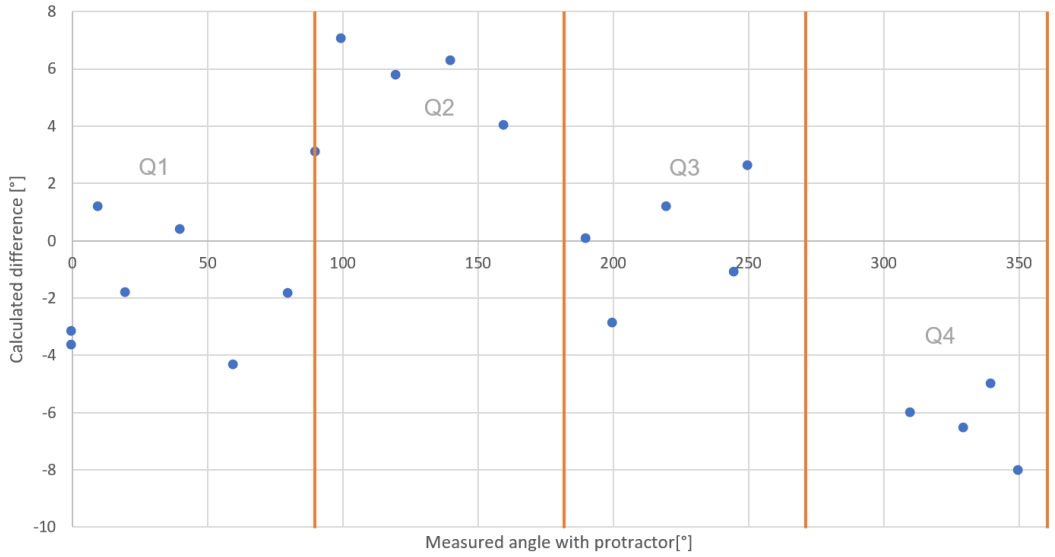

Figure 6.4: The error of the measured value given by the algorithm compared to the measured angle on the protractor. Each value is the mean of five measurements.

The way the angle was measured was far from ideal. The slit embedded into the arms of the prototype did not give a pinpoint angle but rather covered a sector on the protractor. This makes the result somewhat unreliable, but at the same time, it indicates how precise the prototype is at the end of this thesis work and what can be expected if developed in the future. For a better measurement reading a new prototype would be needed in the next iteration.

When the prototype rig was drawn in CAD software, its measurements were carefully reviewed. However, after printing, the crucial measurement of the radius turned out to be different from what was intended. The error was way larger than the tolerance of the 3D-printer, thus a mistake in the design

wasn't noticed during the design review. One of the key benefits of designing a prototype was lost, as the distance from the center to the front edge of the transducer had to be measured with a measuring tape. This issue arises not only due to the design but also because of variations in the transducers' dimensions and their placements. This method is not as accurate as knowing the measurement directly from the design.

6.4 Evaluation of input variables

The variation of the distance reading between transmitter and receiver upon the input parameter r, the radius at which the receiver is placed with respect to the center of the circle, is shown in Figure 6.5. In Figure 6.6, the deviation of the angular measurement is visualised. The spread of the angular variation reduced from $\pm 8°$ to $\pm 6°$ solely by varying the radius r one millimeter. The spread points to the importance of having a very accurate radius of the model to give a fine angle calculation.

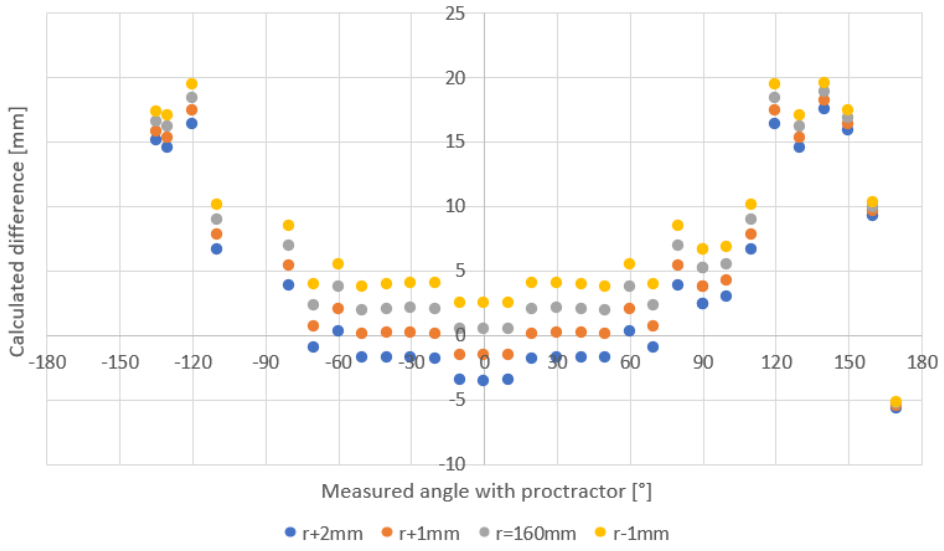

Figure 6.5: The mean of measured error distance reading for T2, with 0° representing the transmitter and receiver being on the opposite side to each other. It also visualises how the result differs when different radii are used in the calculation of an angle.

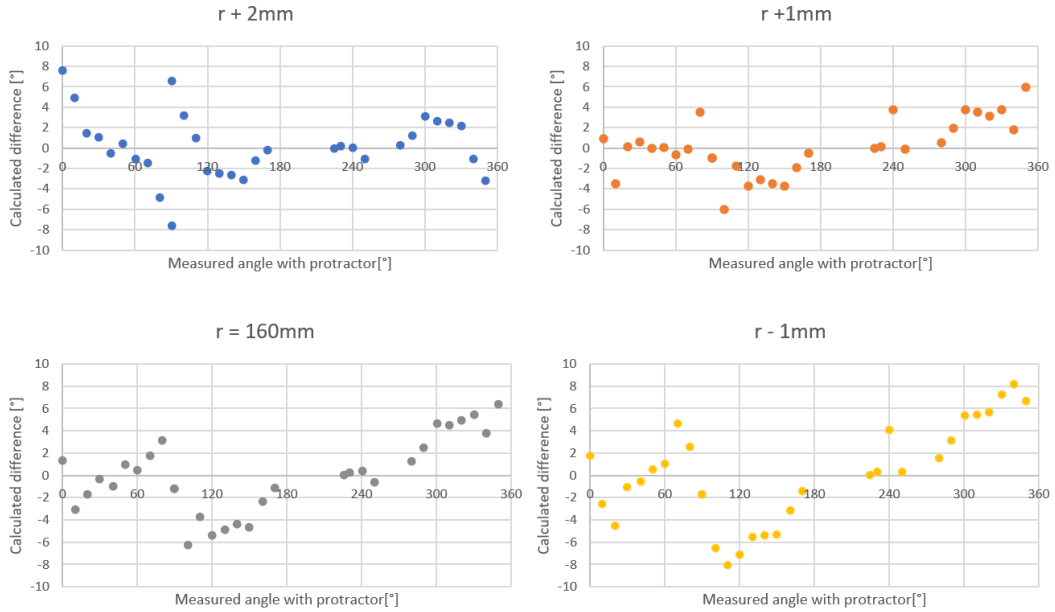

Figure 6.6: The figure show the variation in the measured angle for different receiver position radii.

6.5 Directivity

As figure 6.5 shows, the accuracy of the distance reading depends on the angle between the transmitter and receiver. The dependency can be accounted for by following the path of the sound wave. At higher beam angles, the sound wave enters the transducer at a shallow angle relative to the front plane of the casing. That allows the sound to bounce inside, once or multiple times, before reaching the piezoelectric crystal. This is visualised in figure 6.7. Even though the increase in total distance traveled is not more than a few millimeters, it is a variation large enough to affect the distance reading noticeably.

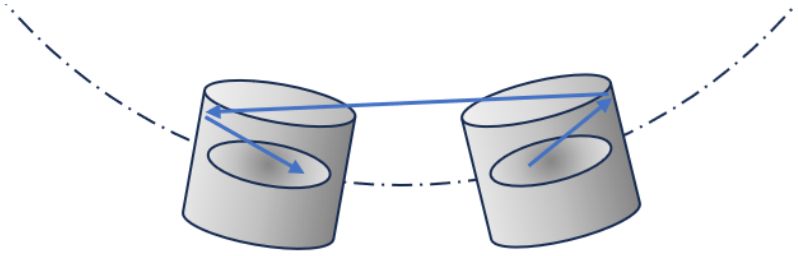

Figure 6.7: The illustration visualises how the sound wave might travel when it enters a casing at a shallow angle.

This additional distance is seen in Figure 6.5 as a significantly increased reading

error at ±70°. The Murata transducers have a directivity set to 80°, which corresponds to an angular position of ±80° for the coordinate system setup used in this concept. The bigger error at ±120° is close to two times the diameter of the transducers with outer dimensions equal to 10 mm. This might indicate that the ultrasonic waves have reflected twice, as illustrated in Figure 6.7. From this, it can be concluded that the spread of the beam angle as well as the transducer's orientation is a limiting factor for angular measurement.

6.6 Evaluation of angular calculation

The calculation of the angle presented in section 2.1 is sensitive to errors in the distance reading, especially at $\theta = 90°n$, where $n = 0, 1, 2, 3$. It is due to the large derivatives of the trigonometric functions at $arcsin(\pm 1)$ and $arccos(\pm 1)$. A small error in the distance reading can lead to a significantly larger error in the angular position. In contrast, a relatively large distance error around $arcsin(0)$ and $arccos(0)$ has minimal impact on the angular position. This can be seen in Figure 6.6 as the spread of the measurements pendulates considerably at $\theta = 0$ and 90°. Similarly, the same sensitivity would apply for the two dead zones, at $\theta = 180$ and 270°.

The great sensitivity at certain angles, alongside the distance error due to echoing inside the case, shows a deficiency in the presented algorithm. In order to determine a more accurate position, this deficiency needs to be taken into consideration. One improvement would be to weigh the different distance readings relative to the knowledge obtained by the results.

6.7 Other analysis

During the development of the prototype one technique wasn't included due to lack of success during implementation. A time estimate of the algorithm was also made, although this is not a core task of the thesis' goal. As these two aren't essential to the developed prototype they are presented in this section.

6.7.1 Time estimate of algorithm

To implement the proposed concept for all four optical modules, the sequence is looped four times, one for each optical module, see chart in Figure 6.8. The total time estimate for the entire algorithm depends on several variables presented in the report. The main time consuming operations are the cross

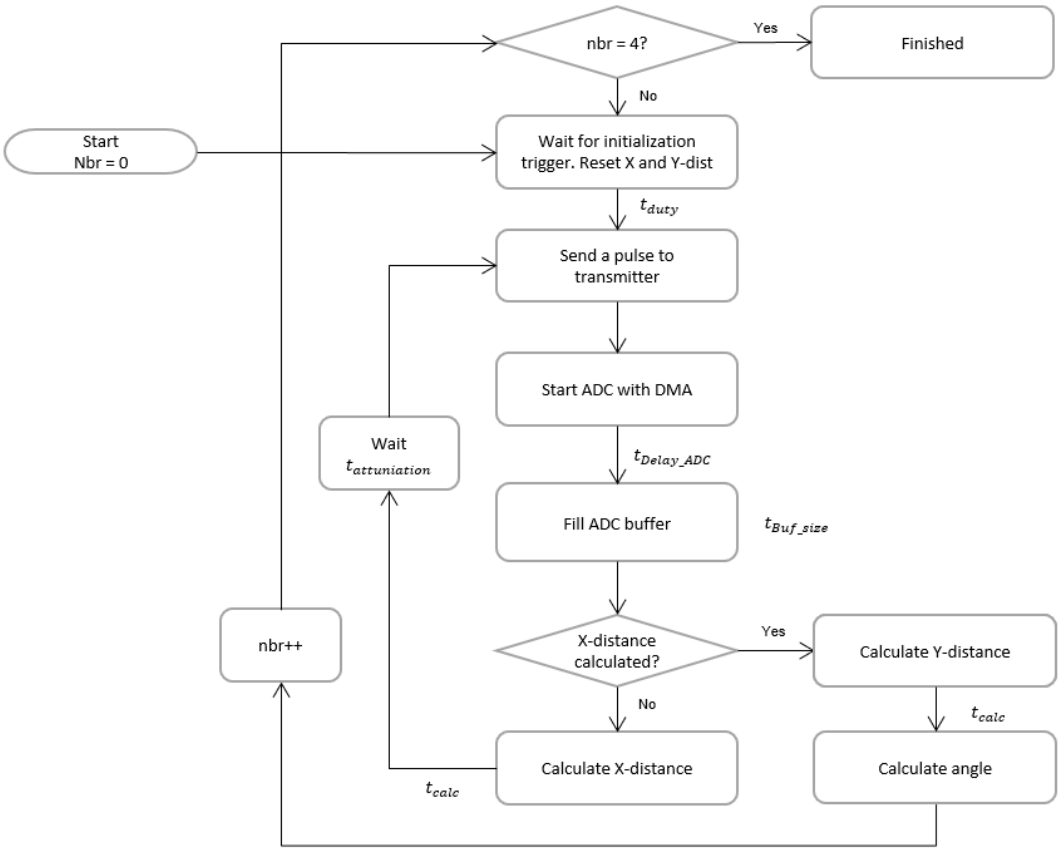

Figure 6.8: The figure shows how the algorithm could be implemented for a system with four optical modules.

correlation calculation and waiting for the sound wave to attenuate. Attenuation time was stated to be a function of the surrounding material in section 3.3.3. The test proved that the ringing is damped after $t_{attenuation} = 3.5ms$. By calculating the cross correlation for the small data set simultaneously as waiting for the attenuation, the operation of all four modules can be performed in some 20ms.

However, the accuracy of the current prototype might require that a series of data is collected and then presented as an average result in case of outliers due to disturbance and noise. This would of course extend the operation time of the algorithm linearly with the number of measurements. If an average of multiple readings is the way to reach a reliable result, 50 measurements of all four modules can still be done in one second. For a human one second is a relatively short time, and if the future developed algorithm requires even more readings, chances are high that it still wouldn't be a time consuming calibration process in the end.

6.7.2 Fast Fourier Transform

When dealing with oscillating functions it can be beneficial to perform a Fourier analysis which gives one the tools to identify and quantify time-based data. Closely related, the Fourier transform decomposes a complex signal into several sinusoidal components, allowing to study the amplitude, frequency and phase. Mathematically, Fourier analysis and transform are applied upon continuous signal, but a digital component, like the ADC in this project, sample data with a given frequency and thus the signal is in the discrete time domain.

This introduces the need to perform a Discrete Fourier Transform (DFT). The DFT is a mathematical operation that converts the data from a time domain into a frequency domain. A Fast Fourier Transform (FFT) is an algorithm that computes the DFT, but does it faster while requiring more memory. FFT has the computing complexity $O(nlog(n))$, where n is the number of samples, compared to DFT with a computing complexity of $O(n^2)$. For large amounts of data, it makes a substantial difference if the faster option is chosen.

Overall, FFT is a fundamental tool in digital signal processing that offers efficiency and is crucial for analyzing frequency components, as for phase shift applications. In the frequency domain, it's possible to enhance the signal by filtering out noise of unwanted frequencies. The disturbance in this project has however mainly been the resonance oscillations due to the direct wave at 40 kHz and can't be filtered away as that is the same frequency as the desired signal. An alternative method for distance measurement, phase shift, was introduced in section 2.5.3, which might produce a more accurate result, although the implementation of it is not as straightforward as ToF.

An attempt to implement FFT, using ARM CMSIS library, as the step before cross correlation was made in this project. Due to a lack of success and time management, the project proceeded with calculation solely in the time domain. The operation may not always be beneficial for small data sets and is therefore left for evaluation if the FFT would reduce the total computational time required.

7 Conclusion and future work

In conclusion, the developed concept for tracking the position of optical modules using ultrasonic waves has achieved an overall accuracy of $\pm 8^\circ$ in position determination, which is far from the product requirement specification, $\pm 0.5^\circ$. Partially, the goal of the thesis has been met which was to investigate and introduce a direct method for position tracking in multi-directional network cameras. The inaccuracy is a consequence of several factors that are presented and discussed throughout the report and are summarized below.

The inaccuracy strongly correlates with poor distance reading that is highly dependent on the angle. Therefore, both the chosen Murata transducer and the orientations of the transducers turned out to be limiting factors. The margin of error in calibration, as well as human factors, have contributed to the position deviation. Furthermore, the current algorithm implementation amplifies the angle error at certain positions within the measurement range, indicating areas for refinement. Finally, the hardware development might not be optimal for filtering out noise and disturbances, such as the direct wave. Due to cost estimations, a transformer drive was eliminated, which might have contributed to the prototype's low robustness.

Reflecting on the thesis objectives, a working prototype was successfully developed, including a signal processing and a distance measurement method customized for the application. Although there are areas for enhancement, this prototype provides a solid foundation for future implementation. The use of ultrasonic measurement, despite the noted challenges, demonstrated good potential for achieving accurate distance readings with affordable components, meeting one of the key goals of the project.

7.1 Future work

The first iteration of the prototype had several delimitations to narrow the scope and establish a foundation for continued development. A few suggestions of potential improvements have been discussed along the time of development. Some of these were not successfully implemented in this prototype and had to be abandoned due to time constraints but still would be interesting to implement and evaluate, and some are things that would change the concept completely up, e.g. the changing transducer model. These ideas of improvement are discussed in the following sections.

7.1.1 ADC

In this implementation, the ADC was set to 12-bit resolution. Whether such high resolution was needed was never investigated in line with the philosophy of development for this thesis. Although, without changing the clock speed of the MCU the sampling frequency can be increased by reducing the resolution of the samples. That is the consequence of one bit resolution equals one ADC clock cycle [25, Sec. 11.7]. The clock speed of the ADC is in turn based upon the speed of the MCU.

It also remains for future development to investigate which parameter has a larger impact on the calculation accuracy: higher ultrasonic frequency or a higher ADC frequency. In theory, a high sampling frequency is the only parameter that needs to be increased as that would lead to less time between samples and thus a higher resolution. One must still be certain that the sampling time is long enough to get an accurate sampling as described in section 4.2. However, when implementing such a solution, it might not work as well as in theory. In that case, increasing the ultrasound frequency could be the way forward. Regardless, if the frequency of ultrasound is increased the sampling frequency also needs to be increased to avoid aliasing and having too few samples per period.

7.1.2 Influence of temperature

As described in section 4.3 and in the background section 2.2.3 the temperature affects the speed of sound and must be considered when doing distance measurements. Another aspect, that was not considered in the development of this thesis, was how the SPL changes in relation to temperature. The reason for that was because the work was done inside a ventilated and air conditioned space. According to the transducer's datasheet (see Appendix B and B.2 for details) the sound pressure level increases by 0.5 dB from 0°C to -40°C and in contrast decreases 2 dB from 0°C to +85°C. In relation to how much the SPL differs when the angle changes, from 0 to -20 dB as seen in figure B.3, this has a small impact. Still, it is something to be considered in the development of a solution that ought to be used outdoors.

7.1.3 Full range

To implement the concept in a multi directional camera, the concept must be able to determine positions in the full 360° range. This project was limited to a two dimensional measuring problem. Additionally, the prototype was constructed with the two transducers positioned on the same radius to eliminate another variable, referring to the angular calculation presented in

section 2.1. With the transducers interacting on the same radius, it is impossible to determine a position where the transmitters are fixed. In addition, it requires the transmitter to have a broad FoV. By solely separating the transmitter and the receiver on two different radii, there is still a possibility for one transducer to block the flight path of another transducer. Full range can be obtained by introducing another parallel plane for the receivers, at the height h. This would mean to implement the equations described in section 2.1. In the three dimensional concept, receiving transducers can be mounted horizontally without blocking the path, facing the transmitter with a 90° angle. On the contrary, this geometric configuration introduces two additional parameters, r_2 and h, which might lead to more uncertainty when measuring a distance and angle.

7.1.4 Additional transmitters

An evident solution to increase the accuracy where the current prototype has weak performance is to simply add more transmitters in corresponding areas. Based on the discussion in section 6.3 about accuracy in quadrants, a third transmitter would probably mean that the overall performance increases, and a fourth even more. How many more transmitters that would be needed to give a good angle reading all around cannot be said without investigating the matter. Introducing several receiver transducers on each optical module and using TDoA is one suggestion to develop the concept. Additionally, letting the optical modules transmit ultrasonic waves, and letting a set of receiving transducers be positioned on the offsetted plane is another suggestion. However, it must not be forgotten though that price is always a relevant factor for products which in this case means a trade-off between performance and cost. This is why a more refined algorithm probably is a cheaper way to achieve the goal of accuracy mentioned in product specification, see section 1.3. A possible solution to this is elaborated below in section 7.1.5.

7.1.5 Potential transducers

For this project, the Murata transducers underwent rigorous testing to assess the performance within the specified parameters for the concept. While evaluating this concept, it becomes imperative to scrutinize alternative transducers suitable for the intended application. Of particular interest are transducers manufactured utilizing MEMs technology, presented in section 2.1. Upon examining the market once more, and broadening the search parameters beyond the prototype constraints, the CH101-02ABR emerged as a promising sensor candidate for further development of the concept.

The CHIRP sensor is an ultrasonic ToF range sensor manufactured by Chirp

Microsystems [26]. The sensor integrates a PMUT with an ultra-low-power SoC (system on chip) in a compact packaging, of size 3.5 X 3.5 x 1.26 mm. The system has an integrated MCU that provides distance measurements reading through an incorporated ultrasonic DSP algorithm. The CH101-02ABR is customized for pitch-catch applications, and operates at 175 kHz allowing for millimeter accurate measurements in the operating range from 4 cm to 1.2 m. Additionally, the sensor can provide up to 100 range samples per second and the transducer can have a customized FoV, up to 180°. Notably, the CHIRP sensor is offered at an affordable cost.

As the next step in the concept development, the CHIRP sensor distance measurement would be introduced. The low power supply, the miniature dimensions and the affordable price are all beneficial for incorporating the concept into a bigger system. The sensor would eliminate the need for both transmitter and receiver circuits as everything is integrated into the sensor. Only the synchronization and angular calculations are required by the MCU. Some compensation for temperature affecting the speed of sound might also be required. Of course, the distance reading needs to be evaluated for the dimensions set up by the refined concept. However, further refinement of the signal is challenging to achieve as the signal processing is embedded in the sensor.

Bibliography

[1] E. Hammar and P. Sjöstrand, "Development of detachable audio accessory for surveillance cameras", M.S. thesis, LTH, Lund University, Lund, Sweden, 2023. [Online]. Available: `https://lup.lub.lu.se/student-papers/search/publication/9136553`.

[2] P. Hoskins, K. Martin and A. Thrush, *Diagnostic Ultrasound*, 3rd ed. Boca Raton, FL: CRC Press/Taylor & Francis Group, 2019.

[3] G. Lindstedt, "Borrowing the bat's ear for automation - ultrasonic measurements in an industrial environment", Ph.D. dissertation, LTH, Lund University, Lund, Sweden, 1996.

[4] W. Moebs, S. J. Ling and J. Sanny, *University physics volume 1*, (Accessed: 2024-02-06), 2016. [Ebook]. [Online]. Available: `https://openstax.org/books/university-physics-volume-1/pages/1-introduction`.

[5] F. Honarvar and A. Varvani-Farahani, "A review of ultrasonic testing applications in additive manufacturing: Defect evaluation, material characterization, and process control", *Ultrasonics*, vol. 108, Dec. 2020. [Online]. Available: `https://www.sciencedirect.com/science/article/pii/S0041624X20301669`.

[6] W. W. L. Au, "Introduction: A comparison of the sonar capabilitites of bats and dolphins", in *Echolocation in Bats and Dolphins*, J. A. Thomas, C. F. Moss and M. Vater, Eds., Chicago, IL: The University of Chicago Press, 2003, ch. Introduction, pp. xiii–xxvi.

[7] J. Hernandez and C. Bleakley, "Low-cost, wideband ultrasonic transmitter and receiver for array signal processing applications", *IEEE Sensors Journal*, vol. 11, no. 5, pp. 1284 –1292, Oct. 2010. [Online]. Available: `https://ieeexplore.ieee.org/document/5604268`.

[8] A. Whitehead, "Ultrasonic driver", *Texas Instruments*, Dec, 6, 2020. [Online video], (Accessed: 2024-03-21). [Online]. Available: `https://www.ti.com/video/series/precision-labs/ti-precision-labs-ultrasonic-sensing.html`.

[9] Y. Yan *et al.*, "Electrostatic sensors – their principles and applications", *Measurement*, vol. 169, Oct. 2020. [Online]. Available: `https://www.sciencedirect.com/science/article/pii/S0263224120310344`.

[10] M. S. Salim, M. Abd Malek, R. Heng, K. Juni and N. Sabri, "Capacitive micromachined ultrasonic transducers: Technology and application", *Journal of Medical Ultrasound*, vol. 20, no. 1, pp. 8–31, Mar. 2012. [Online]. Available: https://www.sciencedirect.com/science/article/pii/S0929644112000094.

[11] J. Perez-Lorenzo, R. Viciana-Abad, P. Reche-Lopez, F. Rivas and J. Escolano, "Evaluation of generalized cross-correlation methods for direction of arrival estimation using two microphones in real environments", *Applied Acoustics*, vol. 73, no. 8, pp. 698–712, Mar. 2012. [Online]. Available: https://www.sciencedirect.com/science/article/pii/S0003682X12000278.

[12] F. Gueuning, M. Varlan, C. Eugene and P. Dupuis, "Accurate distance measurement by an autonomous ultrasonic system combining time-of-flight and phase-shift methods", in *Quality Measurement: The Indispensable Bridge between Theory and Reality (No Measurements? No Science! Joint Conf. - 1996: IEEE Instrumentation and Measurement Technology Conf. and IMEKO Tec*, Brussels, Belgium: IEEE, 1996, pp. 1236–1240. [Online]. Available: https://ieeexplore.ieee.org/document/507414.

[13] H. L. Sneha, "Understanding correlation", *AllAboutCircuits*, Jan. 4, 2017, (Accessed: 2024-06-07). [Online]. Available: https://www.allaboutcircuits.com/technical-articles/understanding-correlation/.

[14] "Avståndsmätare ultraljud hc-sr04 2 - 400cm", *Electrokit*, (Accessed: 2024-04-29). [Online]. Available: https://www.electrokit.com/avstandsmatare-ultraljud-hc-sr04-2-400cm?gad_source=1&gclid=CjwKCAjwkJm0BhBxEiwAwT1AXB_6NoMo8X1FdlebgYl8M_xLU3bBqdT1jh5nx5zxH1X4dSmP1ilxYBoCZMgQAvD_BwE#prodDocuments.

[15] *+5V-Powered, Multichannel RS-232 Drivers/Receivers*, Rev. 18, Analog Devices, Inc., Wilmington, MA, 2019.

[16] *STM32F401xD STM32F401xE, Datasheet*, Rev. 3, STMicroelectronics, Plan-les-Ouates, Switzerland, 2015.

[17] R. C. AB, *Stmicroelectronics stm32 nucleo-64 mcu development board nucleo-f401re*, 2024. [Online]. Available: https://se.rs-online.com/web/p/microcontroller-developmenttools/8029425.

[18] "Analog-to-digital converters basics", *Arrow Electronics, Inc*, Apr. 17, 2023, (Accessed: 2024-05-23). [Online]. Available: https://www.arrow.com/en/research-and-events/articles/engineering-resource-basics-of-analog-to-digital-converters.

[19] B. Wittenmark, K. J. Åström and K.-E. Årzén, *Computer Control: An Overview Educational Version*. Lund, Sweden: Department of Automatic Control, Lund Institute of Technology, 2021.

[20] C. BasuMallick, "What is direct memory access (dma)? meaning, types, principles, working, and benefits", *Spiceworks*, Mar. 14, 2024, (Accessed: 2024-06-07). [Online]. Available: `https://www.spiceworks.com/tech/hardware/articles/direct-memory-access/`.

[21] *ULTRASONIC SENSOR: CUSA-TR60-06-2200-W68*, CUI Devices, Lake Oswego, OR, 2022.

[22] *Data sheet ma40s4s/ma40s4r*, Rev. 2, Murata Manufacturing Co., Ltd., Kyoto, Japan, 2017.

[23] *Application note ma40s4s/ma40s4r*, Rev. 2, Murata Manufacturing Co., Ltd., Kyoto, Japan, 2021.

[24] R. Hedlund and M. Romner, "Ultrasonic positioning system for electric road system", M.S. thesis, LTH, Lund University, Lund, Sweden, 2016. [Online]. Available: `http://lup.lub.lu.se/student-papers/record/8894834`.

[25] *Rm0368 reference manual*, Rev. 5, STMicroelectronics, Plan-les-Ouates, Switzerland, 2018.

[26] *Ch101 ultra-low power integrated ultrasonic time-of-flight range sensor*, Rev. 1.4, Chirp Microsystems, Berkely, CA, 2020.

Appendix A

Microcontroller setting

These are the settings the MCU was configured with in this thesis.

Table A.1: Modified configurations and settings for functions implemented on the MCU

Function	**Configuration and Mode**	**Parameter value**
Core	Clock speed	76.8 MHz
ADC	Resolution	12 bit (15 ADC Clock cycles)
	Continuous Conversion Mode	Enabled
	Channel	10
	Sampling Time	28 Cycles
DMA	DMA Request	ADC1
	Stream	DMA2 Stream 0
	Direction	Peripheral to memory
	Priority	Low
	Increment address	Yes
GPIO	PA2	USART2 TX
	PA3	USART2 RX
	PA5	Green LED
	PA6	TIM3_CH1
	PA7	TIM3_CH2
	PA8	TIM1_CH1
	PA9	TIM1_CH2
	PC8	WireTrigger_TIM3
	PC13	Hardware Trigger TIM1
TIM1	Slave Mode	Trigger Mode
	Trigger Source	TI2FP2
	Clock Source	Internal Clock
	Channel 1	Output Compare CH1
	One Pulse Mode	Yes
	Counter Period	1930-1
	Trigger Polarity	Falling Edge
	Pulse	965-1
	OCMode	TIM_OCMODE_PWM2
TIM3	Slave Mode	Trigger Mode
	Trigger Source	TI1FP1
	Clock Source	Internal Clock
	Channel 2	Output Compare CH2
	One Pulse Mode	Yes
	Counter Period	1930-1
	Trigger Polarity	Falling Edge
	Pulse	965-1
	OCMode	TIM_OCMODE_PWM2

Appendix B

Ultrasonic sensor characteristics

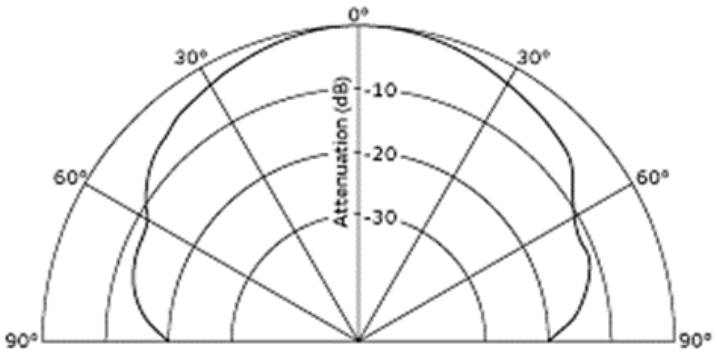

Figure B.1: Directivity in SPL for MA40S4S [22].

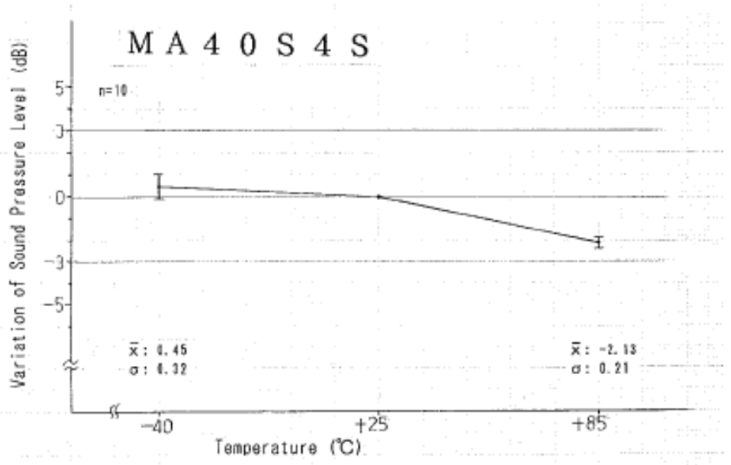

Figure B.2: Sound Pressure Level characteristic of MA40S4S in correlation with temperature [23].

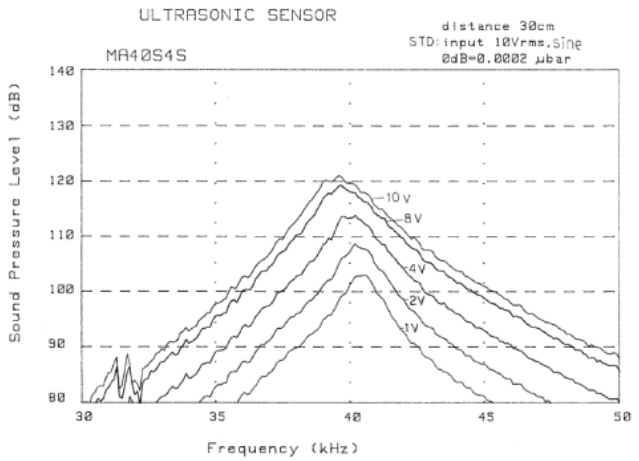

Figure B.3: Sound Pressure Level characteristic of MA40S4S (input voltage dependency) [23].